Affinity requirements for control of synaptic targeting and neuronal cell survival by heterophilic IgSF cell adhesion molecules

Shuwa Xu[1]*, Alina P Sergeeva[2], Phinikoula S. Katsamba[3], Seetha Mannepalli[3], Fabiana Bahna[3], Jude Bimela[3], S. L. Zipursky[4], Lawrence Shapiro[3,5], Barry Honig[2,3,5,6], Kai Zinn[1]*

[1]California Institute of Technology, Division of Biology and Biological Engineering, Pasadena, CA,
[2]Department of Systems Biology, Columbia University Medical Center, New York, NY 10032, USA
[3]Zuckerman Mind Brain and Behavior Institute, Columbia University, New York, NY 10027, USA
[4]Department of Biological Chemistry, HHMI, David Geffen School of Medicine, University of California, Los Angeles, Los Angeles, CA 90095, USA
[5]Department of Biochemistry and Molecular Biophysics, Columbia University, New York, NY 10032, USA
[6]Department of Medicine, Columbia University, New York, NY 10032, USA

*Corresponding authors:
Shuwa Xu (shuwaxu@caltech.edu), Kai Zinn (zinnk@caltech.edu).

SUMMARY

Neurons in the developing brain express many different cell adhesion molecules (CAMs) on their surfaces. CAM binding affinities can vary by more than 200-fold, but the significance of these variations is unknown. Interactions between the immunoglobulin superfamily CAM DIP-α and its binding partners Dpr10 and Dpr6 control synaptic targeting and survival of *Drosophila* optic lobe neurons. We designed mutations that systematically change interaction affinity and analyzed function *in vivo*. Reducing affinity causes loss-of-function phenotypes whose severity scales with the magnitude of the change. Synaptic targeting is more sensitive to affinity reduction than is cell survival. Increasing affinity rescues neurons that would normally be culled by apoptosis. By manipulating CAM expression together with affinity, we showed that the key parameter controlling circuit assembly is surface avidity, which is the strength of adherence between cell surfaces. We conclude that CAM binding affinities and expression levels are finely tuned for function during development.

INTRODUCTION

Synapses in the central nervous systems of both vertebrates and invertebrates reside within dense and complex neuropils. During the development of “hard-wired” neural systems such as the *Drosophila* brain, axonal and dendritic processes choose genetically specified synaptic targets within environments where they have access to the surfaces of many non-target neurons. Roger Sperry’s chemoaffinity hypothesis proposed that individual neurons in such systems are labeled by molecules that give them unique identities. The modern version of this hypothesis is that cell adhesion molecule (CAM)-like cell surface proteins (CSPs) expressed on interacting neuronal surfaces bind to each other and trigger downstream events that cause establishment of synaptic connections between appropriate partners.

CAM-like CSPs involved in synaptic targeting, which are denoted as cell recognition molecules (CRMs), include immunoglobulin superfamily (IgSF) proteins, cadherin superfamily proteins, leucine-rich repeat proteins, teneurins, and others. Some of these proteins bind homophilically, some have unique heterophilic partners, and still others bind to a variety of partners (Honig and Shapiro, 2020; Sanes and Zipursky, 2020). Each *Drosophila* neuron can express 100 or more different CAM genes during development (Barish et al., 2018; Konstantinides et al., 2018; Kurmangaliyev et al., 2019, 2020; Li et al., 2020; Özel et al., 2021; Tan et al., 2015). The number in vertebrates is comparable (Sarin et al., 2018). Many studies have shown that loss, overexpression, or misexpression of CAMs can change synaptic connectivity.

Most CAM interactions are of relatively low affinity, with dissociation constants (K_Ds) in the μM range. By contrast, secreted protein ligands often bind to their receptors with nanomolar K_Ds. Large variations in affinity exist even among CAMs in the same protein family. For example, type I and type II cadherins interact both homophilically and heterophilically, and their K_Ds can vary by over

100-fold (Shapiro & Honig 2020). It is interesting to speculate that CAM binding affinity constitutes another mechanism for control of wiring specificity. However, the *in vivo* functions of affinity variation have not been investigated.

The “Dpr-ome” interaction network was discovered in an *in vitro* “interactome” screen of IgSF CSPs(Özkan et al., 2013). Twenty-one Dpr proteins interact in a complex pattern with 11 DIPs (Carrillo et al., 2015; Cosmanescu et al., 2018; Tan et al., 2015). Most DIPs bind to multiple Dprs, and *vice versa*. In the pupal optic lobe (OL), neurons expressing a particular DIP are often postsynaptic to neurons expressing a Dpr to which that DIP binds *in vitro* (Carrillo et al., 2015; Cosmanescu et al., 2018; Tan et al., 2015). Loss of DIPs and Dprs can alter synaptic connectivity and cause neuronal death, indicating that these proteins are CRMs(Sanes and Zipursky, 2020)(Ashley et al., 2019; Barish et al., 2018; Bornstein et al., 2021; Carrillo et al., 2015; Cheng et al., 2019; Courgeon and Desplan, 2019; Menon et al., 2019; Venkatasubramanian et al., 2019; Xu et al., 2019, 2018). The binding affinities of all interacting DIP/Dpr pairs have been measured using biophysical methods, and K_Ds for homophilic and heterophilic binding vary by more than 100-fold, ranging from <2 μM to >200 μM(Cosmanescu et al., 2018).

DIP-α binds to two closely related Dpr partners, Dpr10 and Dpr6, with some of the highest affinities within the Dpr-ome (K_Ds of ≤2 μM) (Cosmanescu et al., 2018; Sergeeva et al., 2020) (Figure 1). DIP-α is expressed in several classes of neurons in the medulla of the pupal OL, including Dm4 and Dm12, which arborize in the M3 layer. The L3 lamina neuron is presynaptic to Dm4 and Dm12, and expresses both Dpr10 and Dpr6 (Figure 2A) (Davis et al., 2020; Kurmangaliyev et al., 2020; Tan et al., 2015; Xu et al., 2018). Loss of interactions between DIP-α and its Dpr partners causes several phenotypes, including Dm4 and Dm12 cell loss, ectopic projection of Dm12 processes to the M8 layer, and alteration of Dm12 synapse number. Ectopic overexpression of Dpr10 in the M10 layer of the medulla causes Dm4 and Dm12 neurons to arborize in M10 (Xu et

al., 2018). This provides an ideal system in which to study the significance of affinity for a heterophilic CRM binding pair that controls multiple developmental processes.

To understand how affinity affects CAM function *in vivo*, it is important to separate the effects of affinity alterations from those of protein expression level. We introduced a series of designed mutations that either decrease or increase binding affinity into the *DIP-α* and *dpr10* loci, so that the mutant proteins would be expressed under the control of endogenous regulatory elements. We observed that reducing affinity causes loss-of-function (LOF) phenotypes, and that the severity of these phenotypes scales with the magnitude of affinity reduction. Synaptic targeting and cell survival have different affinity requirements.

Increasing affinity does not alter targeting, but affects cell survival. Our results suggest that DIP-α::Dpr10 engagement controls a trophic support pathway that counteracts cell death pathways. When DIP-α::Dpr10 interactions are sufficiently strengthened, the culling of visual system neurons by apoptosis that occurs during wild-type development is eliminated. Changes in gene expression levels can compensate for alterations in protein binding affinity, indicating that avidity is the key parameter that determines the outcome of interactions between neurons mediated by these CAMs. The affinities and expression levels of DIP-α and its Dpr partners appear to be tuned so that the correct number of neurons survive and form appropriate synaptic connections.

RESULTS

Generation and selection of DIP-α and Dpr10 mutations that change DIP-α::Dpr10 binding affinity

DIP-α binds to two Dprs, Dpr10 and Dpr6, with affinities of 1.4 μM and 2.0 μM, respectively. DIP-α also binds to itself with an affinity of 24 μM (Cheng et al., 2019; Cosmanescu et al., 2018; Sergeeva et al., 2020). We developed computational approaches that allowed the design of DIP-α and Dpr10 mutants that changed DIP-α::Dpr10 binding affinity *in vitro* (Sergeeva et al., 2020). To determine how changes in affinity affect neuron-neuron recognition events, we selected a set of DIP-α and Dpr10 mutations for *in vivo* studies based on the following criteria: 1) the mutations should alter binding affinity between DIP-α and Dpr10 in a graded fashion, so as to generate a set of proteins with affinities varying over a wide range; 2) the mutations should not change their specificity for binding to other DIP/Dpr proteins; 3) the mutations should not have strong effects on the homophilic binding affinity of DIP-α.

Based on these criteria, we chose the designed DIP-α mutants K81Q (K_D=31.8 μM, *DIP-α^{-20F}*; the superscripts in mutant names indicate the direction and fold change in affinity relative to wild-type), K81Q G74S (K_D=68.0 μM, *DIP-α^{-50F}*), and G74A (K_D=0.9 μM, *DIP-α^{+2F}*); and Dpr10 mutants V144K (K_D=11.3 μM, *dpr10^{-8F}*) and Q138D (K_D=27.6 μM, *dpr10^{-20F}*). To achieve a greater affinity range, we designed two additional Dpr10 mutants, V144K Q142E G99D (K_D=50.0 μM, *dpr10^{-40F}*) and Q142M (K_D= 0.19 μM, Dpr10^{+10F}) (Figures 1B, C). K_D is further decreased to 0.10 μM (a ~20-fold increase in affinity relative to wild-type) when DIP-α^{+2F} binds to Dpr10^{+10F}. The locations of the designed mutations in the DIP-α::Dpr10 interface are indicated in Figure 1A.

These Dpr10 and DIP-α mutations did not change the specificity of their binding to other DIP/Dpr proteins. Figure 1B shows binding isotherms for interactions of

Dpr10 wild-type and mutant proteins with DIP-α, DIP-β and DIP-γ (see Figure S1 for corresponding sensorgrams). DIP-β is closest to DIP-α among all other DIPs in sequence, and is also a Dpr10 binding protein, but with a much lower affinity (K_D=33 μM). DIP-γ is not a Dpr10 binding protein (K_D >1000 μM). Like wild-type Dpr10, all three mutant Dpr10 proteins interact more strongly with DIP-α than with DIP-β, and do not bind to DIP-γ (Figure 1B). Figure 1C shows binding isotherms for DIP-α wild-type and mutant proteins to Dpr10, Dpr4, Dpr7 and Dpr12 (see Figure S1 for corresponding sensorgrams). Like wild-type DIP-α, none of the DIP-α mutants exhibits measurable binding to Dpr4, Dpr7, or Dpr12, which are members of non-cognate Dpr subgroups (Figure 1C).

Dpr10 is a monomer, while DIP-α can form dimers *in vitro* with a K_D of 24 μM (Cosmanescu et al., 2018). The DIP-α/DIP-α and Dpr10/DIP-α interfaces are very similar (RMSD of 0.6Å), and hence changes in the surface used for heterophilic binding by DIP-α would be expected to also alter the homophilic DIP-α/DIP-α interface. To ensure that the DIP-α mutants retained the ability to homodimerize, we measured homophilic binding affinities of all DIP-α mutants using analytical ultracentrifugation (AUC). The homophilic binding K_Ds for the three DIP-α mutant proteins are: DIP-α G74A (*DIP-α*$^{+2F}$), K_D=50 μM; DIP-α K81Q (*DIP-α*$^{-20F}$) K_D=19.6 μM; DIP-α K81Q G74S (*DIP-α*$^{-50F}$) K_D=46 μM (Table S1). All mutants remain dimeric, and homophilic binding affinity is changed by no more than 2-fold. In summary, we have successfully created Dpr10 and DIP-α mutants with a wide affinity range that do not affect cognate binding preferences of DIPs and Dprs relative to non-cognate partners.

DIP-α and Dpr10 affinity mutants are expressed normally *in vivo*

We introduced the chosen mutations into the endogenous *DIP-α* and *dpr10* genomic loci by a precise CRISPR mediated knock-in strategy (Zhang et al., 2014). We tested expression *in vivo* using antibodies specific for DIP-α and Dpr10 (Figures 2B, C). Wild-type DIP-α is expressed in three neuropil layers in

the medulla region of the OL during mid-pupal development (48h after puparium formation/APF) (Xu et al., 2018) (Figures 2B'). All DIP-α affinity mutants were localized to the medulla neuropil and expressed in the same layers as wild-type (Figures 2B''-B''''). The DIP-α-expressing Dm1, Dm4 and Dm12 neurons project to the first (M1) and second (M3) DIP-α expressing layers (Figures 2A, B'). A large fraction of these neurons undergo cell death during pupal development in *DIP-α* null mutants (Xu et al., 2018). If our introduced mutations caused LOF phenotypes, they would be expected to cause a reduction in staining intensity in these two layers due to cell death, even if they do not alter the levels of expression in individual cells. Another set of DIP-α expressing neurons that project to a third layer (M10; yellow dotted line in Figure 2B') do not exhibit detectable cell death in null mutants, so we quantitated the expression levels of DIP-*α* mutant proteins in this layer. All three alleles showed similar expression levels to wild-type DIP-α in M10 (Figure 2D).

Dpr10 is expressed in two major medulla layers in the 48h APF optic lobe (Figure 2C'). All three Dpr10 affinity mutant proteins were expressed in the wild-type pattern (Figures 2C''-C''''). Since no Dpr10-expressing OL neurons are known to exhibit cell death, we quantified Dpr10 expression levels in the whole neuropil. Two Dpr10 alleles were expressed at the same level as the wild-type ($Dpr10^{-8F}$ and $Dpr10^{-40F}$), while one was expressed at a slightly higher level than wild-type ($Dpr10^{-20F}$) (Figure 2E).

Reducing DIP-α::Dpr10 affinity causes graded mistargeting of Dm12 neurons

Null *DIP-α* mutations or *dpr6 dpr10* double-null mutations disrupt targeting of Dm12 neurons and reduce survival of Dm1, Dm4 and Dm12 neurons (Xu et al., 2018). To determine how changing binding affinity between DIP-α and Dpr10 affects these processes, we first analyzed targeting of Dm12 neurons. Previously, we showed that $DIP\text{-}\alpha^{null}$ Dm12 clones in a wild-type background target to a more proximal medulla layer, M8 (Figures 3B, G) (Xu et al., 2018). To better quantitate and visualize mistargeting in affinity mutants, we modified our

methodologies by changing the genetic background and altering permeabilization, which allowed us to examine much larger numbers of neurons using whole-animal mutants (see Experimental Procedures). In *DIP-α*^{null} mutants, about one-third of Dm12 neurons (~43 per OL) mistargeted to M8 (Figures 3B, G, M). In *DIP-α*$^{-20F}$, which has a ~20-fold reduction in DIP-α::Dpr10 binding affinity, ~5 (4%) of Dm12 neurons per OL mistargeted to M8 (Figures 3C, M). This number increased to ~20 (17%) in *DIP-α*$^{-50F}$, which reduces affinity by ~50 fold (Figures 3D, M).

Dpr10 and Dpr6 are both expressed in L3, which forms synapses with Dm12 and Dm4 (Figure 2A). Loss of both Dprs (in a double-null mutant) causes the same mistargeting and cell death phenotypes seen in *DIP-α* null mutants. *dpr10* or *dpr6* single mutants have much weaker phenotypes, indicating that the Dprs have partially redundant functions (Xu et al., 2018). Thus, to facilitate the analysis of the relationships between Dpr10 affinity and function, we knocked *dpr10* affinity mutations into the endogenous *dpr10* locus in a *dpr6* null mutant background. We analyzed Dm12 neurons in the three *dpr10* affinity mutants described above (*dpr10*$^{-8F}$, *dpr10*$^{-20F}$, and *dpr10*$^{-40F}$). Animals expressing only wild-type Dpr10, but not Dpr6 (*dpr6*^{null} single mutant) displayed a mild mistargeting phenotype in Dm12 neurons, with on average ~8 mistargeted Dm12 neurons per OL (Figures 3H, M). When Dpr10 affinity to DIP-α was reduced by 8-fold (in *dpr6*^{null} *dpr10*$^{-8F}$), ~14 mistargeted Dm12 neurons were observed (Figures 3I, M). A further reduction in affinity to 20-fold less than wild-type (*dpr6*^{null} *dpr10*$^{-20F}$) caused a doubling of the number of mistargeted neurons, to ~29 cells (Figures 3J, M). Thus, in both *dpr10* and *DIP-α* mutants, the severity of Dm12 mistargeting scales with DIP-α:Dpr10 affinity reduction.

In these experiments, we observed that *dpr10* mutations that reduce affinity by 20- or 40-fold had stronger phenotypes than *DIP-α* mutations that reduce affinity by 20- or 50-fold (Figure 3M). However, as described above, *dpr10* affinity mutations were knocked into a *dpr6* null background, while *DIP-α* affinity mutant phenotypes were analyzed in a wild-type *dpr6* background. Because Dpr6 and

Dpr10 are partially redundant (Xu et al., 2018), to accurately assess the relationships between phenotypic severity and DIP-α::Dpr10 binding affinity we analyzed Dm12 neurons in *DIP-α* affinity mutants that also lack Dpr6. The presence of the $dpr6^{null}$ mutations increased the extent of Dm12 mistargeting observed in *DIP-α* affinity mutants. For example, in the *DIP-α* mutant that decreases DIP-α::Dpr10 affinity by 20-fold, the number of mistargeted Dm12 neurons per OL increased from ~5 in $DIP\text{-}\alpha^{-20F}$ to ~24 in $DIP\text{-}\alpha^{-20F}$ $dpr6^{null}$ (Figures 3E, M). This number is similar to that observed in the *dpr10* affinity mutant that also reduces DIP-α::Dpr10 affinity by 20-fold ($dpr6^{null}$ $dpr10^{-20F}$: ~29). In conclusion, in the absence of Dpr6, comparable phenotypic severity is observed for *DIP-α* or *dpr10* mutants that change DIP-α::Dpr10 affinity by a similar extent (Figure 3M).

Different affinity thresholds control Dm12 targeting and cell survival

There are ~115 Dm12 neurons in a wild-type OL. In *DIP-α* or *dpr6 dpr10* null mutants, about 25 of these (~22%) die during development, reducing the total Dm12 complement to ~90 (Figure 3N) (Xu et al., 2018). Reducing DIP-α::Dpr10 binding affinity by 20-fold in a wild-type *dpr6* background did not cause any cell loss ($DIP\text{-}\alpha^{-20F}$). However, in the absence of Dpr6 ($DIP\text{-}\alpha^{-20F}$ $dpr6^{null}$), ~9 Dm12 cells are lost. Removing Dpr6 from $DIP\text{-}\alpha^{-50F}$ mutants produces a further increase in Dm12 cell loss, from ~9 to ~17 (Figure 3N). *dpr10* affinity mutants are examined in a *dpr6* null mutant background, and ~8 Dm12 cells are lost in *dpr6* single mutants. This number is not significantly changed by addition of $dpr10^{-8F}$ or $dpr10^{-20F}$ affinity mutations. However, in $dpr6^{null}$ $dpr10^{-40F}$ mutants, ~24 cells are lost (Figure 3N). Thus, in the absence of Dpr6 a 40- to 50-fold reduction in DIP-α::Dpr10 binding affinity produces a null or near-null cell loss phenotype.

These results indicate that mistargeting and cell loss have different dependencies on DIP-α::Dpr10 binding affinity. We first observe a significant increase in mistargeting when affinity (K_D) is reduced to 11.3 μM, in $dpr6^{null}$ $dpr10^{-8F}$. When affinity is reduced by ~20-fold, in either $dpr6^{null}$ $dpr10^{-20F}$ (K_D=27.8

μM) or *DIP-α*$^{-20F}$ *dpr6*^{null} (K_D=31.8 μM), the penetrance of the mistargeting phenotype is about 50% of that observed in null mutants (Figures 3M, O). For cell loss, no increase above the *dpr6* null mutant penetrance is observed for *DIP-α*$^{-20F}$ or *dpr6 dpr10*$^{-20F}$ mutants. A threshold of ~50% of the null penetrance is first exceeded in *dpr6*^{null} *dpr10*$^{-40F}$ (K_D=50.0 μM) or *DIP-α*$^{-50F}$ *dpr6*^{null} (K_D=68.0 μM) (Figures 3N, O). Thus, we conclude that the 50% threshold for mistargeting is reached at a K_D of ~30 μM, while the threshold for cell loss occurs at ~50 μM. Note that there is more cell death in *dpr6*^{null} *dpr10*$^{-40F}$ than in *DIP-α*$^{-50F}$ *dpr6*^{null} (Figure 3N). Perhaps in a *dpr6*^{null} background the number of accessible DIP-α molecules on Dm12 processes is in excess of the number of Dpr10 molecules on the axons of L3 and other presynaptic neurons in the M3 layer. This could account for cell survival phenotypes being more sensitive to perturbation of Dpr10.

A reduction in cell survival with decreasing affinity is also observed for Dm4 and Dm1 neurons

Dm4 and Dm1 processes do not mistarget in *DIP-α* null or *dpr6, dpr10* double null mutants (Figures 4A, D, S2) (Xu et al., 2018). This suggests that DIP-α::Dpr10 interactions are redundant with other cues in directing the arbors of Dm4 and Dm1 neurons to the correct layers. However, survival of Dm4 and Dm1 neurons is affected by null *DIP-α* or *dpr6 dpr1*0 mutations, so we were able to examine the effects of affinity mutations on cell survival for Dm4 and Dm1. We observed that Dm4 and Dm1 cell survival is also decreased in affinity mutants, and that their survival is more sensitive to affinity reduction than that of Dm12 neurons. In *DIP-α*$^{-20F}$*/DIP-α*^{null} (null) mutants (wild-type for *dpr6*), cell loss was seen for Dm4 and Dm1, but not for Dm12 (Figures 3N, 4B, 4I, S2). The stronger affinity mutant *DIP-α*$^{-50F}$*/DIP-α*^{null} exhibited as much cell loss as the null allele for Dm4 and Dm1, but had a weaker phenotype than the null for Dm12 (Figures 3N, 4C, 4I, S2). Survival of Dm4 neurons was also more sensitive than survival of Dm12 neurons to affinity reduction by *dpr10* mutations. Dm4 cell loss is observed in *dpr6*^{null} *dpr10*$^{-20F}$ mutants (Figures 4G, J), which have wild-type numbers of

Dm12 neurons (Figure 3N). As for Dm12, *dpr10* affinity mutants have stronger phenotypes than the corresponding *DIP-α* mutants, presumably because Dpr6 is still expressed in these *DIP-α* mutant backgrounds. These data suggest that different cell types have different affinity thresholds for regulation of cell survival. This could be due to different levels of expression of DIP-α in Dm4 and Dm1 neurons as compared to Dm12, and/or to the use of alternative cell death pathways.

Increasing DIP-α::Dpr10 affinity rescues Dm4 cell death

The analysis of affinity reduction mutants described above shows that affinity thresholds exist for neuronal targeting and survival. When affinity is reduced to below these thresholds, neurons exhibit LOF phenotypes. We wished to also examine the consequences of increasing the affinity between DIP-α and Dpr10. Because DIP-α::Dpr10 is already one of the highest affinity interactions in the Dpr-ome, it is difficult to design mutants that increase affinity based on comparisons among DIP::Dpr binding interfaces. However, using position scanning mutagenesis in FoldX (Sergeeva et al., 2020), we were able to predict and experimentally validate two mutants that passed the selection criteria discussed above, DIP-α^{G74A} (K_D=0.90 μM, DIP-α^{+2F}) and $Dpr10^{Q142M}$ (K_D=0.19 μM, $Dpr10^{+10F}$). When DIP-α^{+2F} binds to $Dpr10^{+10F}$, K_D is further decreased to 0.10 μM, which represents a ~20-fold increase in affinity as compared to wild-type (Figures 5A, B).

Dm4, Dm12 and Dm1 exhibited normal layer targeting in both of the two increased affinity mutants (Figures 5C-H, Figure S3). We then analyzed cell death phenotypes in Dm4 neurons. We have shown previously that Dm4 neurons are produced in excess in wild-type animals (~55 cells/OL), and that their number is reduced to ~40 cells/OL by apoptotic cell death during early pupal development (Figures 5I, J) (Xu et al., 2018). When apoptosis inhibitors (either baculovirus p35 protein or the *Drosophila* death-associated inhibitor of apoptosis 1 protein) are expressed in Dm4, the number of Dm4 neurons in adults remains

at ~55 per OL (Figures 5I, J) (Xu et al., 2018). Loss of DIP-α or its Dpr partners causes increased Dm4 cell death, but it was unknown whether the natural Dm4 cell death that occurs in wild-type is also regulated by DIP::Dpr interactions. To evaluate this, we counted adult Dm4 cell number in flies with increased affinity between DIP-α and Dpr10. In flies carrying two copies of *DIP-α*$^{+2F}$, or one copy of *dpr10*$^{+10F}$ over wild-type *dpr10*, there was a small increase in Dm4 number, to ~45-48 cells/OL. Note that, because *dpr10*$^{+10F}$ was knocked into a *dpr6* null background, we analyzed *dpr10*$^{+10F}$ over a wild-type chromosome (*dpr6*^{WT}, *dpr10*^{WT}) to eliminate effects caused by loss of Dpr6, which in theory would counteract the effects of increasing affinity between DIP-α and Dpr10. In flies expressing both DIP-α^{+2F} and Dpr10^{+10F} (*DIP-α*$^{+2F}$*/DIP-α*^{WT}*; dpr10*$^{+10F}$*/dpr10*^{WT}), there were ~55 Dm4 cells per OL, which is equal to the number observed when apoptosis inhibitors are expressed in wild-type (Figures 5I, J). These results suggest that Dm4 cell death is entirely controlled by DIP-α's interactions with its Dpr partners. Apoptosis in wild-type is partially suppressed by a trophic support pathway controlled by trans-synaptic DIP::Dpr interactions. Decreasing trophic support by reducing DIP-α::Dpr10 affinity leads to excess cell death, and increasing trophic support to above wild-type levels by increasing affinity suppresses normal cell death. The affinity and expression levels of DIP-α and its partners, and therefore the extent of apoptosis suppression, may have been adjusted by evolution to produce the desired number of adult Dm4 cells.

An affinity threshold for induction of Dm4 mistargeting by ectopic Dpr10

Ectopic expression of Dpr10 in M10 is sufficient to induce mistargeting of the processes of DIP-α expressing neurons (Xu et al, 2018). To analyze if this instructional role is also dependent on affinity, we made UAS lines for Dpr10 affinity mutants and tested their abilities to induce mistargeting. Both Dm4 and Dm12 neurons displayed misexpression-induced mistargeting (Xu et al., 2018). Because of Dm4's smaller cell number (40 Dm4s *vs*. 115 Dm12s) and thicker mistargeting axon branches, it is easier to quantitatively assess Dm4

mistargeting events. Thus, we used Dm4 neurons for analysis of mistargeting by Dpr10 affinity mutants.

T4 is not a synaptic partner of Dm4, but T4 processes come into contact with neurons that project to other medulla layers during early pupal development. They later segregate into the M10 layer of the medulla (Figure 2A). When endogenous Dpr10 is knocked out, and ectopic Dpr10 is misexpressed at high levels in T4 cells, it causes Dm4 neurons to send their processes to M10, bypassing their normal M3 target layer (Xu et al., 2018). We expressed Dpr10 affinity mutants in M10 using T4-Gal4. Dpr10 antibody staining revealed that M10 layer expression of UAS-Dpr10^{-8F} and UAS-Dpr10^{-20F} is comparable to that of wild-type UAS-Dpr10, while UAS-Dpr10^{-40F} is expressed at 1.6-fold higher levels than wild-type (Figure S4).

We analyzed each affinity mutant protein's ability to induce mistargeting of Dm4 neurons in a *dpr6 dpr10* double null mutant background (Figures 6A-A'', 6B-B''). About half of the Dm4 neurons undergo cell death due to the lack of Dpr6 and Dpr10, and as a result, there are fewer Dm4 processes in M3. The remaining ~20 Dm4 cells all target to the correct layer, so there must be other cues that direct Dm4 processes to M3 in the absence of DIP-α and its Dpr partners (Figures 4A-H) (Xu et al., 2018). When wild-type Dpr10 was expressed in M10, Dm4 cell death was partially rescued (see below), and most of the Dm4 terminals were in the M10 layer, leaving few terminals in M3 (Figures 6C-C''). We counted Dm4 processes leaving M3 and targeting to M10 (Figures 6C-F, yellow arrows), and divided that number by the total number of Dm4 cell bodies in the same sample, which we defined as the percentage of mistargeted Dm4 neurons. It sometimes exceeded 100%, indicating that some Dm4 neurons send out more than one process to the M10 layer (Figure 6G). Expressing Dpr10^{-8F} in M10 caused about half as much Dm4 mistargeting as wild-type Dpr10, while expressing Dpr10^{-20F} or Dpr10^{-40F} produced almost no mistargeting (Figures 6D-H).

We also tested the three Dpr10 affinity variants' abilities to induce Dm4 mistargeting in a wild-type animal, in which endogenous Dpr6 and Dpr10 in M3 compete with exogenous Dpr10 in M10. The percentage of mistargeted Dm4 neurons was reduced in this genetic background, but the three variants' relative ability to induce mistargeting remained the same (Figure 6G). The gain-of-function (GOF) mistargeting phenotype has more stringent affinity requirements than the LOF Dm12 targeting phenotype, because Dpr10^{-8F} (K_D=11.3 μM) induces mistargeting about half as well as wild-type Dpr10, while Dpr10^{-20F} (K_D=27.8 μM) produces no mistargeting. This places the 50% penetrance threshold for this phenotype around 11 μM, while for the LOF phenotype it is at ~30 μM (Figure 3O).

Cell surface avidity is a key parameter controlling circuit assembly

The targeting and trophic support functions of DIP-α::Dpr10 interactions are both mediated through contact between neuronal cell surfaces. The contacting regions can be considered as apposed two-dimensional sheets, each of which contains many DIP or Dpr molecules. The overall affinity of the cell surfaces for each other, known as avidity, is a combination of individual protein-protein binding affinity and protein density. It is likely that avidity determines whether or not the strength of interaction between the two cells is sufficient to produce correct targeting and/or suppress cell death. To examine this issue, we manipulated the expression levels of DIP and Dpr affinity mutants and examined the resulting phenotypes.

In the first set of experiments, we analyzed cell number control in Dm4 neurons, comparing flies carrying one *vs.* two copies of an affinity mutant *DIP-α* gene. Although ~6 Dm4 cells were rescued from cell death in *DIP-α*$^{+2F}$*/DIP-α*$^{+2F}$ flies, there was no change in Dm4 cell number in *DIP-α*$^{+2F}$*/DIP-α*$^{-}$ animals (Figures 5I, 7A). In mutants that reduce affinity (*DIP-α*$^{-20F}$ and *DIP*$^{-50F}$), there were significant differences in Dm4 number between animals with two copies of a mutant gene *vs.* those with one mutant copy over a null (Figure 7A). Thus, Dm4 cell number is

affected by *DIP-α* gene expression level, implying that avidity determines trophic support levels. Removing a copy of wild-type *DIP-α* did not alter Dm4 cell number (Figure 7A), suggesting that the phenotype is buffered around the wild-type condition. This may be a general phenomenon that explains why haploinsufficiency is rare in *Drosophila* and most LOF mutations are recessive.

To examine whether expression levels affect neuronal targeting as well, we analyzed Dm12 mistargeting phenotypes in animals bearing one or two copies of wild-type or affinity mutant *dpr10* genes. Removing one copy of wild-type *dpr6* and one copy of wild-type *dpr10* produced no phenotypes (Figure S5A). In $dpr6^{null}/dpr6^{null}$ (null) animals (bearing two copies of wild-type *dpr10*), there are on average ~8 Dm12 neurons that mistarget to M8. Loss of one copy of wild-type *dpr10* in the *dpr6* null mutant background produced a significant increase in mistargeting, with ~20 Dm12 cells mistargeting to M8 (Figure S5A). In $dpr10^{null}/dpr10^{null}$ (null) animals (bearing two copies of wild-type *dpr6*), ~31 Dm12 neurons mistarget to M8, so mistargeting is more sensitive to the loss of Dpr10 than to loss of Dpr6. Loss of one copy of wild-type *dpr6* in the *dpr10* null mutant background did not further increase mistargeting (Figure S5A). For affinity mutants, *dpr6* null mutant animals with one copy of $dpr10^{-8F}$ had stronger phenotypes than those with two copies (22 *vs*. 14 mistargeted axons, respectively) (Figure S5A). However, there were no copy number effects for $dpr10^{-20F}$ or $dpr10^{-40F}$. In Figure 3M, we showed that there is a large (~2-fold) change in phenotypic penetrance between $dpr10^{-8F}/dpr10^{-8F}$ and $dpr10^{-20F}/dpr10^{-20F}$, so mistargeting is likely sensitive to avidity alteration within that affinity range. However, $Dpr10^{-20F}$ is at the 50% penetrance affinity threshold, and $Dpr10^{-40F}$ is below that threshold, so copy number changes for these alleles may have little effect. In conclusion, for both Dm4 cell number control and Dm12 targeting, two-fold changes in gene copy number can have strong effects on phenotype in certain mutants, suggesting that the avidity of the interactions between the L3 and Dm4/Dm12 cell surfaces determines the functional consequences of these interactions.

Overexpression of Dpr10 mutants can compensate for reduced protein binding affinity

The results described above indicate that *dpr10* LOF phenotypes are affected both by altering binding affinity and by changing avidity through alteration of gene expression levels through copy number changes. To further examine this issue, we asked whether overexpressing Dpr10 affinity mutants could compensate for reduction in individual protein-protein binding affinity. *dpr10*$^{-20F}$ and *dpr10*$^{-40F}$ mutants both showed significant Dm4 cell loss. We overexpressed these mutant Dpr10 proteins in Dm4's synaptic partner, the L3 neuron, and analyzed rescue of Dm4 cell loss. We had previously shown that overexpressing wild-type Dpr10 in L3 fully rescues Dm4 cell loss in *dpr6*^{null} *dpr10*^{null} mutants (Xu et al., 2018). When we overexpressed Dpr10^{-20F} or Dpr10^{-40F} in L3, they fully rescued Dm4 cell loss in *dpr6*^{null} *dpr10*$^{-20F}$ or *dpr6*^{null} *dpr10*$^{-40F}$, respectively, and were also able to rescue the *dpr6*^{null} *dpr10*^{null} phenotype (Figures 7B, S5B). These results show that increasing protein amounts can indeed compensate for reductions in individual protein-protein binding affinity (Figure 7C). Interestingly, they also indicate that our affinity mutants would have been classified as fully functional using conventional Gal4 rescue.

Finally, to test whether these results are specific to the Dm4 synaptic partner L3, we overexpressed different UAS-Dpr10 variants in T4 neurons, which project to M10. When wild-type Dpr10 was expressed in T4 cells, it was able to rescue cell loss due to the *dpr6 dpr10* double mutation, but not fully to the wild-type number (34 *vs*. 40)(Xu et al., 2018). Dpr10^{-20F} or Dpr10^{-40F} were able to rescue Dm4 cell number to similar extents as wild-type Dpr10 (Figure S5C). The fact that rescue of Dm4 neuronal survival by T4-Gal4 is not complete even for wild-type Dpr10 could be due to the fact that the T4-Dm4 interaction is transient. Alternatively, there may be other proteins on the L3 surface that contribute to cell survival that are missing from T4 neurons. Note also that induction of Dm4 mistargeting by expression of Dpr10 in T4 cells has stringent affinity requirements (Dpr10^{-20F}

cannot induce mistargeting)(Figure 6H), while T4>Dpr10^{-20F} works as well as wild-type to rescue Dm4 cell death. This is likely because, in order to induce mistargeting, T4>Dpr10 must override the other cues that cause Dm4 to arborize in M3. By contrast, to rescue cell death, it is only necessary to supply enough Dpr10 signaling to replace that provided by the normal interaction between L3 and Dm4, and this can be done by increasing the expression levels of low affinity mutants.

DISCUSSION

In this paper, we systematically explore the impact of CAM affinity and avidity on synaptic connectivity in the *Drosophila* brain, focusing on the Dm4 and Dm12 medulla neurons, which are postsynaptic to the L3 lamina neuron in medulla layer M3. Dm4 and Dm12 express DIP-α, and L3 expresses its binding partners Dpr10 and Dpr6. The loss of interactions between DIP-α and its Dpr partners causes death of Dm4 and Dm12 neurons and mistargeting of Dm12 processes from layer M3 to layer M8 (Xu et al., 2018). To examine how alterations in DIP-α::Dpr10 binding affinity affect targeting and cell survival, we introduced designed affinity mutations into the endogenous *DIP-α* and *dpr10* loci in the background of a *dpr6* null mutation, so that the mutant proteins would be expressed at endogenous levels. We made fly lines expressing DIP-α mutants that bound to Dpr10 with ~20 and ~50-fold decreases in affinity relative to wild-type, as well as a mutant with a ~2-fold increase in affinity. Dpr10 lines expressed mutants that bound to DIP-α with ~8, ~20, and ~40-fold decreases, and a ~10-fold increase in affinity (Figures 1, 2).

Affinity requirements for synaptic targeting

Targeting of Dm12 processes to M3, the medulla layer in which these neurons form synapses, is perturbed by mutations that reduce DIP-α::Dpr10 binding affinity. In LOF mutants, Dm12 processes mistarget to M8 (Figure 3). Since Dpr6 and Dpr10 have partially redundant functions(Xu et al., 2018), to obtain an accurate estimate of the affinity threshold for targeting, we needed to examine both *dpr10* and *DIP-*α mutants in a *dpr6* null background. When we did this, we observed that a severity of ~50% of the null penetrance is observed when DIP-α::Dpr10 affinity is reduced from 1.4 μM (wild-type) to ~30 μM (Figure 3M).

Ectopic expression of Dpr10 in T4 neurons causes Dm12 and Dm4 processes to mistarget to M10 (Xu et al., 2018). We examined affinity requirements for this GOF phenotype using Dm4, because mistargeting is easier to quantitate for this

neuron. Dm4 mistargeting through ectopic expression has more stringent affinity requirements than the LOF Dm12 mistargeting phenotype, because Dpr10^{-8F} (K_D=11.3 μM) is only ~50% as effective as wild-type Dpr10, and Dpr10^{-20F} (K_D=27.8 μM) does not cause mistargeting (Figure 6H). This may be because there are other cues that direct Dm4 processes to M3 in the absence of DIP-α and Dpr10 (null mutations cause no Dm4 mistargeting), and ectopic Dpr10 expressed in M10 must overcome these cues in order to induce mistargeting.

Affinity requirements for Dm12 cell survival and targeting are different

To evaluate Dm12 cell survival, we counted Dm12 neurons in the same LOF genotypes used for examination of targeting. We found that survival has less stringent affinity requirements. The threshold of 50% of the null penetrance is only reached when affinity is reduced to ≤50 μM (Figure 3N). Targeting and cell survival may use different downstream signaling components, accounting for the differential sensitivity of these phenotypes to affinity reduction. The signaling pathways downstream of DIP-α are likely to be mediated by unknown cell surface proteins, since DIP-α has no cytoplasmic domain (Özkan et al., 2013). Our preliminary analysis suggests that DIP-α is attached to the membrane by a glycosyl-phosphatidylinositol (GPI) linkage (data not shown).

DIP-α::Dpr10 affinity is finely tuned for control of Dm4 cell number

About 20% of the Dm4 cells that are originally generated are culled by apoptosis during early pupal development. There are ~40 Dm4 cells in a wild-type OL, but ~55 cells are present in adults if Dm4 apoptosis is blocked. In *DIP-α* null or *dpr6 dpr10* double-null mutants, ~50% of the remaining Dm4 neurons die, leaving ~20 cells in adults. This produces gaps in arbor coverage (Xu et al., 2018). Reducing affinity produces a gradual reduction in Dm4 cell number, and the severity of cell loss scales with the magnitude of affinity reduction (Figure 4).

Increasing DIP-α::Dpr10 affinity by ~20-fold rescues all of the cells that undergo

apoptosis in wild-type (Figure 5). We conclude that the affinity of DIP-α::Dpr10 interactions is finely tuned to maintain an adult Dm4 cell assembly of ~40. When DIP-α on Dm4 binds to Dpr10, it activates a trophic support pathway that counteracts apoptosis, and DIP-α::Dpr10 interaction strength controls how much trophic support Dm4 neurons will receive. The balance between apoptosis and trophic support determines how many Dm4 neurons will survive to adulthood. Since Dm4 neurons tile the medulla, the lateral extent of their arborizations within layer M3, and thus the sizes of their receptive fields, is inversely proportional to the number of Dm4 cells, and hence dependent on the affinities of DIP-α::Dpr6/10 interactions.

Similar mechanisms might apply to another medulla neuron, Dm8, which also tiles the medulla. DIP-γ is expressed on a subset of Dm8 neurons (yDm8), and its partner Dpr11 is on presynaptic yR7 photoreceptors. yDm8 survival and dendritic morphology are controlled by DIP-γ::Dpr11 interactions. About 1/3 of yDm8 cells are culled by apopotosis during wild-type development, and these cells are rescued if more trophic support is supplied by expressing Dpr11 on all R7s (Menon et al., 2019)(Courgeon and Desplan, 2019).

Extensive programmed cell death occurs in the OL during wild-type pupal development (Togane et al., 2012), and many OL neuron types are produced in excess. The affinities of binding between presynaptic and postsynaptic CRMs might control cell number coordination in the developing visual system, ensuring that peripheral neurons in the retina and lamina are paired with the proper number of processing center neurons in the medulla. Each neuronal type could use a single pair of interacting CRMs to both direct synaptic targeting and determine cell number.

Relationships between avidity and affinity

We altered avidity while keeping individual protein-protein binding affinity fixed by changing the copy number of affinity mutant chromosomes and by

overexpressing and/or misexpressing affinity mutants. These alterations in expression level, timing, and patterning can have strong effects on the extent of cell death and mistargeting. For example, genotypes with one copy of *DIP-α*$^{-20F}$ over a null *DIP-α* mutation have significant Dm4 cell loss, while no cell loss is observed for *DIP-α*$^{-20F}$/*DIP-α*$^{-20F}$ (Figure 7). It is likely that DIP-α protein levels are altered by ~2-fold when gene copy number is changed, but we have not directly demonstrated this. A copy number effect on Dm12 mistargeting is observed for *dpr10*$^{-8F}$, but not for *dpr10*$^{-20F}$ and *dpr10*$^{-40F}$, which already produce near-null phenotypes when present in two copies (Figure S5).

We examined rescue of reduced affinity mutants by Gal4-driven overexpression of the same mutants, and found that an increase in protein level was able to fully compensate for the reduction of individual protein-protein interaction affinity (Figure 7). Reduced affinity proteins can also fully rescue null phenotypes when overexpressed (Figure S5). This illustrates the importance of introducing mutations into endogenous genes in order to assay subtle changes in protein function: increasing avidity through overexpression can allow even low-affinity mutants to behave like wild-type alleles, which will mask the functional changes in these mutant proteins.

Affinity variation in CAM interactions and nervous system assembly.

Many previous studies have examined the effects of removing CAMs and altering CAM expression levels, and the results suggest that the summed affinity (avidity) of interactions between neuronal surfaces is important for the organization of nervous system elements. For example, all lamina neurons express a single cadherin, CadN, and the concentric organization of the lamina cartridge is controlled by the relative levels of CadN. L1 and L2 neurons at the center of the cartridge express the highest levels of CadN, and R cells at the periphery express it at low levels. Manipulating CadN expression can change the relative positions of the neurons within the cartridge and alter its pattern of synapses (Schwabe et al., 2014). Similar mechanisms exist in the medulla (Trush et al.,

2019).

The functions of binding affinities among individual CSPs have been examined in the immune system. For example, the affinities of interactions between T-cell receptors and their peptide–major histocompatibility complex ligands control T-cell specificities and activities (for review, see Stone, 2009). In the nervous system, however, the significance of CAM binding affinity has not been extensively studied. One paper examined affinity mutants of the SYG-1 and SYG-2 CAMs in *C. elegans*, which controls formation of synapses between motor neurons and muscles. Overexpressed SYG-1 mutant proteins with reduced affinity for SYG-2 are impaired in their ability to rescue the *syg-1* null mutant, suggesting that SYG-1::SYG-2 binding affinity is important for function (Özkan et al., 2014). These results differ from our observations with DIP-α::Dpr10, for which overexpression of low affinity mutants fully rescued LOF phenotypes. The differences could be due to the strength of the drivers used for overexpressing proteins in *C.elegans* vs. *Drosophila*.

Given the large number of CAMs expressed by a given neuron and the large variations in affinity among these CAMs (Kurmangaliyev et al, 2019, 2020; Li et al, 2017; Tan et al, 2015; Ozel et al, 2021), it is likely that the affinities of individual CAM binding pairs have been selected by evolution. The Dpr-ome has seven specificity groups, each of which contains one to three DIPs that interact with one to five Dprs (Figure S1)(Carrillo et al., 2015; Cosmanescu et al., 2018; Sergeeva et al., 2020). The DIP-α group contains DIP-α, Dpr10, and Dpr6, and is a high affinity interaction group, with K_Ds of ≤2 μM. The other two DIP::Dpr interactions that have been shown to be essential for brain wiring thus far, DIP-γ::Dpr11 and DIP-δ::Dpr12, are also of relatively high affinity (Bornstein et al., 2021; Carrillo et al., 2015; Courgeon and Desplan, 2019; Menon et al., 2019). By contrast, in the DIP-η/θ/ι and DIP-ε/ζ groups, all K_Ds are >22 μM. Three of the five Dprs in the DIP-η/θ/ι group have no interactions with DIPs that have K_Ds of less than 70 μM, which would represent a null mutant phenotype for Dpr10

(Figure S1C). This raises the question of whether these interactions might have different functions than those in the high affinity groups.

Neurons form transient interactions with many other cells during axon/dendrite outgrowth and synaptogenesis. Some transient interactions, such as those with guidepost cells and intermediate targets, are genetically specified and help to determine the correct pattern of synaptic connections. Others probably occur randomly as a consequence of the dense packing of the developing neuropil. The ability of cells to form and break transient interactions may be facilitated by having a variety of CAMs with μM affinity on their surfaces, each of which is present in many copies. This could allow cells to manipulate the strengths of their adhesive interactions with intermediate targets by modulating the levels of multiple CAMs that have partners on those targets. By contrast, if cells interacted with each other *via* a small number of copies of a few CAMs with much higher affinities, one or more CAMs might have to be completely removed in order to allow a neuron to break a transient interaction with an intermediate target.

Affinity alterations change the rates of association and/or dissociation of CAM complexes, and these rates might in turn affect the kinetics of transient associations between neuronal surfaces during development. It will be interesting to determine whether the lower affinities of the DIP-η/θ/ι and DIP-ε/ζ groups, which might affect neuronal interactions with intermediate targets, are important for function, and if increasing affinity for these DIPs will cause defects in wiring. In our future work, we hope to address the mechanisms through which affinity and avidity control CAM signaling for other binding pairs in the OL and other areas of the nervous system.

METHOD DETAILS

Generation of affinity mutant flies

DIP-α^{+2F}, DIP-α^{-20F} and DIP-α^{-40F}: The genomic sequence of *DIP-α* including exon2-exon4 was first replaced with the sequence of attP-3XP3-DsRed-attP using a CRISPR-based knock-in strategy (Zhang et al., 2014), generating *DIP-α*-PRP flies. The same *DIP-α* genomic region was amplified from the wild-type fly genome using PCR and cloned into pBS-attB vector to make the donor plasmid. Mutations (G74A, K81Q, K81Q+G74S) that change DIP-α binding affinity to Dpr10 were introduced into the donor plasmid. Donor plasmids were injected into *DIP-α*-PRP flies generated above. Through ΦC31 recombinase-mediated cassette exchange, mutations were introduced into the fly genome (Injection completed at Bestgene. Inc). The detailed procedure was as in Zhang, *et.al.* 2014.

Dpr10^{-8F}, Dpr10^{-20F} Dpr10^{-40F}: First, in Vas-Cas9(X);+/+;*dpr6*^{null} flies, the genomic sequence of *dpr10* including 2 exons encoding the first Ig domain of dpr10 was replaced with the sequence of attP-3XP3-DsRed-attP using a CRISPR-based knock-in strategy (Zhang et al., 2014), generating *dpr6*$^{-}$, *dpr10*-PRP flies. The same *dpr10* genomic region was amplified from the wild-type fly genome and cloned into pBS-attB vector to make the donor plasmid. Mutations (Q138D, V144K, G99D+Q142E+V144K) that change Dpr10 binding affinity to DIP-α were introduced into the donor plasmid. Donor plasmids were injected into *dpr6*$^{-}$, *dpr10*-PRP flies generated above. Through ΦC31 recombinase-mediated cassette exchange, mutations were introduced into the fly genome (Injection completed at Bestgene. Inc). The detailed procedure was as in Zhang, *et.al.* 2014.

Generation of UAS-transgenic flies

cDNA encoding DIP-α-RA and Dpr10-RD were cloned into the pJFRC28 vector (Pfeiffer et al., 2012) using standard cloning methods. The V5 sequence was

inserted after signal peptide and before Ig1 for DIP-α and Dpr10 as described in (Xu et al., 2018). Mutations that change DIP-α and Dpr10 affinity (*DIP-α*: G74A, K81Q, K81Q+G74S; *dpr10*: Q138D, V144K, G99D+Q142E+V144K) were cloned into the above plasmids. Transgenes were inserted into the specific landing site at 28E7 by injection of fertilized embryos (Bestgene, Inc.). Plasmid and primer design were carried out using the software Snapgene. Plasmids and detailed sequences are available upon request.

Immunohistochemistry

Fly brains were dissected in PBS (137mM NaCl, 2.7mM KCl, 10mM Na2HPO4, 1.8mM KH2PO4) and fixed in PBS with 4% paraformaldehyde for 30 min at room temperature (RT). After 3 rinses with PBT at RT, samples were incubated in PBT (PBS 0.5% Triton-X100) containing 5% normal goat serum plus 5% normal donkey serum (blocking solution) for at least 1hr at RT. To visualize fine processes of mis-targeted Dm12 neurons, fly brains were fixed in PBT plus 4% paraformaldehyde to increase tissue permeability. Brains were incubated at 4°C in primary and secondary antibodies for at least one day each with multiple PBT rinses at RT in between and afterwards. Brains were mounted in EverBrite mounting medium (Biotium).

The following primary antibodies were used in this study: chicken-anti-GFP (1:1000, Abcam ab13970); rabbit-anti-RFP (1:500, Clontech 600-401-379); mouse-anti-24B10 (Zipursky et al., 1984) (1:20, DSHB); mouse-anti-Brp (nc82) (1:10, DSHB); chicken-anti-V5 (1:500, Abcam 9113); mouse-anti-V5 (1:200, Life Technology, R96025); mouse-anti-DIP-α (4G11) (1:20) (Xu et al., 2018), mouse-anti-Dpr10 (1:5000) (Xu et al., 2018).

Secondary antibodies were used at 1:500 dilutions. From Jackson ImmunoResearch Lab: Alexa Fluor 488 donkey-anti-chicken (703-545-155); Alexa Fluor 488 donkey-anti-mouse (715-545-151); Alexa Fluor 594 donkey-anti-rabbit (711-585-152); From ThermoFisher Scientific: Alexa Fluor 647 goat-anti-

mouse (A28181); Alexa Fluor 568 goat-anti-mouse (A-11004). From Life Technologies: Alexa Fluor 647 donkey-anti-mouse (A-21236).

Microscopy and Image Analysis

Confocal images were acquired on a Zeiss LSM880 confocal microscope. The staining patterns were reproducible between samples. However, some variation on the overall fluorescence signal and noise levels existed between sections and samples. Thus, proper adjustments of laser power, detector gain, and black level settings were made to obtain similar overall fluorescence signals.

Quantification of fluorescence intensity (in Figure 2, Figure 5): Samples were mounted dorsal up. For each sample, 15 slices of confocal images were taken starting from 50 μm away from the surface, at 5 μm step size. Each slice is analyzed separately against background signal for fluorescence intensity in ROI.

Surface Plasmon Resonance (SPR) binding experiments

SPR binding assays were performed using a Biacore T100 biosensor equipped with a Series S CM4 sensor chip. To minimize artificial binding resulting from enhanced- avidity effects of oligomers binding to an immobilized ligand surfaces, DIPs are consistently used as ligands and immobilized over independent flow cells using amine-coupling chemistry in HBS pH 7.4 (10mM HEPES, 150mM NaCl) buffer at 25°C using a flow rate of 20 μL/min. Dextran surfaces were activated for 7 minutes using equal volumes of 0.1M NHS (N-Hydroxysuccinimide) and 0.4M EDC(1-Ethyl-3-(3-dimethylaminopropyl) carbodiimide). Each protein of interest was immobilized at ~30μg/mL in 10 mM sodium acetate, pH 5.5 until the desired immobilization level was achieved. The immobilized surface was blocked using a 4-minute injection of 1.0 M ethanolamine, pH 8.5. Typical immobilization levels ranged between 760-980 RU. To minimize nonspecific binding the reference flow cell was blocked by immobilizing BSA in 10 mM sodium acetate, pH 4.25 for 3 minutes using a similar amine-coupling protocol as described above.

Binding analysis was performed at 25°C in a running buffer of 10 mM Tris-HCl, pH 7.2, 150mM NaCl, 1mM EDTA, 1 mg/mL BSA and 0.01% (v/v) Tween-20. Dpr analytes were prepared in running buffer and tested at nine concentrations using a three-fold dilution series ranging from 81-0.012 μM. Similarly, Dpr10 was tested over the DIP-α and DIP-α G74A-immobilized surfaces at eight concentrations using a three-fold dilution series ranging from 27-0.012 μM. Dpr10 Q138D was also tested at a concentration range of 27-0.012 μM over all DIP surfaces, due to a limited protein expression of this mutant. In each experiment, every concentration was tested in duplicate. During a binding cycle, the association phase between each analyte and the immobilized molecule was monitored for either 30 or 40 seconds as indicated by the plotted sensorgrams, followed by 120-second dissociation phase, each at 50 μL/min. At the end of the dissociation phase the signal returned to baseline thus eliminating the need for a regeneration step. The last step was buffer wash injection at 100 μL/min for 60 seconds. The analyte was replaced by buffer every two or three binding cycles to double-reference the binding signals by removing systematic noise and instrument drift. The responses between 25 and 29 seconds, at which point the binding reactions achieve equilibrium as observed by the flat binding responses, were plotted against the concentration of analyte. The data was fit to 1:1 interaction model and the K_D was calculated as the analyte concentration that would yield 0.5 R_{max} (Rich and Myszka, 2009). The data was processed using Scrubber 2.0 (BioLogic Software).

QUANTIFICATION AND STATISTICAL ANALYSIS

Images were analyzed with ImageJ software. Cell number counting were facilitated with Fiji (Schindelin et al., 2012) plugin “ClearVolume” (Royer et al., 2015) and Imaris (Bitplane Inc) software (semi-automatically with hand-correction). Statistical analysis was done using Prism software. All data are shown as mean ± standard deviation (SD). Statistical test: unpaired t-test.

TRANSGENIC ANIMALS USED IN THIS STUDY

D. melanogaster: 24F10-GAL4	Bloomington Drosophila Stock Center	BDSC 49090, RRID:BDSC_49090
D. melanogaster: 75F06-GAL4	Bloomington Drosophila Stock Center	BDSC 39901, RRID:BDSC_39901
D. melanogaster: 23G11-LexA	Bloomington Drosophila Stock Center	BDSC 54775, RRID:BDSC_54775
D. melanogaster: 24F10-LexA	Bloomington Drosophila Stock Center	BDSC 52696, RRID:BDSC_52696
D. melanogaster: 75F06-LexA	Bloomington Drosophila Stock Center	BDSC 54100, RRID:BDSC_54100
D. melanogaster: 47G08-GAL4	Bloomington Drosophila Stock Center	BDSC 50328, RRID:BDSC_50328
D. melanogaster: 47G08-LexA	Bloomington Drosophila Stock Center	BDSC 52793 RRID: BDSC_50328
D. melanogaster: 15E02-GAL4	Bloomington Drosophila Stock Center	BDSC 48691, RRID:BDSC_48691
D. melanogaster: 9B08-GAL4	Bloomington Drosophila Stock Center	BDSC 41369, RRID:BDSC_41369
D. melanogaster: 42F06-GAL4	Bloomington Drosophila Stock Center	BDSC 41253, RRID:BDSC_41253
D. melanogaster: 9D03-GAL4	Bloomington Drosophila Stock Center	BDSC 47364, RRID:BDSC_47364
D. melanogaster: 9-9-GAL4	(Nern et al., 2008)	FlyBase FBti0141173
D. melanogaster: 13xLexAop-CD4-tdTom (attp2)	(Xu, et. al., 2018)	N/A
D. melanogaster: 10xUAS-myr::GFP (attP2; attP40)	(Xu, et. al., 2018)	N/A
D. melanogaster: LexAop-myr::GFP	(Xu, et. al., 2018)	N/A
D. melanogaster: LexAopmyrtdTomato	(Xu, et. al., 2018)	N/A
D. melanogaster: UAS-FSF-myrGFP	(Xu, et. al., 2018)	N/A
D. melanogaster: hs-Flp:PEST	Bloomington Drosophila Stock Center	BDSC 77141, RRID:BDSC_77141
D. melanogaster: *DIP-α*^{GAL4} (MI02031)	(Xu, et. al., 2018)	N/A
D. melanogaster: *DIP-α*$^{-}$ (*DIP-α*^{null})	(Xu, et. al., 2018)	N/A
D. melanogaster: *dpr6*$^{-}$ (*dpr6*^{null})	(Xu, et. al., 2018)	N/A
D. melanogaster: *dpr10*$^{-}$ (*dpr10*^{null})	(Xu, et. al., 2018)	N/A
D. melanogaster: *dpr6-10*$^{-}$ (*dpr6-10*^{L})	(Xu, et. al., 2018)	N/A

D. melanogaster: UAS-Dpr10D.NV5	(Xu, et. al., 2018)	N/A
D. melanogaster: UAS-Dpr6F.NV5	(Xu, et. al., 2018)	N/A
D. melanogaster: UAS-DIP-α.NV5	(Xu, et. al., 2018)	N/A
D. melanogaster: *DIP-α^{+2F}*	This paper	N/A
D. melanogaster: *DIP-α^{-20F}*	This paper	N/A
D. melanogaster: *DIP-α^{-50F}*	This paper	N/A
D. melanogaster: *Dpr10^{-8F}*	This paper	N/A
D. melanogaster: *Dpr10^{-20F}*	This paper	N/A
D. melanogaster: *Dpr10^{-40F}*	This paper	N/A
D. melanogaster: UAS-DIP-α^{-20F}	This paper	N/A
D. melanogaster: UAS-DIP-α^{-50F}	This paper	N/A
D. melanogaster: UAS-Dpr10^{-8F}	This paper	N/A
D. melanogaster: UAS-Dpr10^{-20F}	This paper	N/A
D. melanogaster: UAS-Dpr10^{-40F}	This paper	N/A
Genotypes of all animals used in this study are provided in supplemental table S1.		

ACKNOWLEDGEMENTS

We thank Richard Mann Lab for general discussions. Confocal imaging was completed in the Caltech Biological Imaging Facility. This work was supported by Kai Zinn's NIH grants R37 NS028182 and RO1 NS096509; and Barry Honig's NSF grant MCB-1914542.

Reference:

Ashley, J., Sorrentino, V., Lobb-Rabe, M., Nagarkar-Jaiswal, S., Tan, L., Xu, S., Xiao, Q., Zinn, K., and Carrillo, R.A. (2019). Transsynaptic interactions between IgSF proteins DIP-α and Dpr10 are required for motor neuron targeting specificity. Elife *8*, e42690.

Barish, S., Nuss, S., Strunilin, I., Bao, S., Mukherjee, S., Jones, C.D., and Volkan, P.C. (2018). Combinations of DIPs and Dprs control organization of olfactory receptor neuron terminals in Drosophila. PLOS Genet. *14*, e1007560.

Bornstein, B., Meltzer, H., Adler, R., Alyagor, I., Berkun, V., Cummings, G., Reh, F., Keren‐Shaul, H., David, E., Riemensperger, T., et al. (2021). Transneuronal Dpr12/DIP‐δ interactions facilitate compartmentalized dopaminergic innervation of *Drosophila* mushroom body axons. EMBO J. e105763.

Carrillo, R.A., Özkan, E., Menon, K.P., Nagarkar-Jaiswal, S., Lee, P.-T., Jeon, M., Birnbaum, M.E., Bellen, H.J., Garcia, K.C., and Zinn, K. (2015). Control of Synaptic Connectivity by a Network of Drosophila IgSF Cell Surface Proteins. Cell *163*, 1770–1782.

Cheng, S., Ashley, J., Kurleto, J.D., Lobb-Rabe, M., Park, Y.J., Carrillo, R.A., and Özkan, E. (2019). Molecular basis of synaptic specificity by immunoglobulin superfamily receptors in Drosophila. Elife *8*, e41028.

Cosmanescu, F., Katsamba, P.S., Sergeeva, A.P., Ahlsén, G., Patel, S.D., Brewer, J.J., Tan, L., Xu, S., Xiao, Q., Nagarkar-Jaiswal, S., et al. (2018). Neuron-Subtype-Specific Expression, Interaction Affinities, and Specificity Determinants of DIP/Dpr Cell Recognition Proteins. Neuron *100*, 1385–1400.

Courgeon, M., and Desplan, C. (2019). Coordination between stochastic and deterministic specification in the Drosophilavisual system. Science (80-.). *366*, eaay6727-13.

Honig, B., and Shapiro, L. (2020). Adhesion Protein Structure, Molecular Affinities, and Principles of Cell-Cell Recognition. Cell *181*, 520–535.

Konstantinides, N., Kapuralin, K., Fadil, C., Barboza, L., Satija, R., and Desplan, C. (2018). Phenotypic Convergence: Distinct Transcription Factors Regulate Common Terminal Features. Cell *174*, 622-635.e13.

Kurmangaliyev, Y.Z., Yoo, J., Locascio, S.A., and Lawrence Zipursky, S. (2019). Modular transcriptional programs separately define axon and dendrite connectivity. Elife *8*, e50822.

Kurmangaliyev, Y.Z., Yoo, J., Valdes-Aleman, J., Sanfilippo, P., and Zipursky, S.L. (2020). Transcriptional Programs of Circuit Assembly in the Drosophila Visual System. Neuron *108*, 1045-1057.e6.

Li, J., Han, S., Li, H., Udeshi, N.D., Svinkina, T., Mani, D.R., Xu, C., Guajardo, R., Xie, Q., Li, T., et al. (2020). Cell-Surface Proteomic Profiling in the Fly Brain Uncovers Wiring Regulators. Cell *180*, 1–14.

Menon, K.P., Kulkarni, V., Takemura, S., Anaya, M., and Zinn, K. (2019). Interactions between Dpr11 and DIP-γ control selection of amacrine neurons in Drosophila color vision circuits. Elife *8*, e48935.

Nern, A., Zhu, Y., and Zipursky, S.L. (2008). Local N-cadherin interactions mediate distinct steps in the targeting of lamina neurons. Neuron *58*, 34–41.

Özel, M.N., Simon, F., Jafari, S., Holguera, I., Chen, Y.C., Benhra, N., El-Danaf, R.N., Kapuralin, K., Malin, J.A., Konstantinides, N., et al. (2021). Neuronal diversity and convergence in a visual system developmental atlas. Nature *589*, 88–95.
Özkan, E., Carrillo, R.A., Eastman, C.L., Weiszmann, R., Waghray, D., Johnson, K.G., Zinn, K., Celniker, S.E., and Garcia, K.C. (2013). An Extracellular Interactome of Immunoglobulin and LRR Proteins Reveals Receptor-Ligand Networks. Cell *154*, 228–239.
Pfeiffer, B.D., Truman, J.W., and Rubin, G.M. (2012). Using translational enhancers to increase transgene expression in Drosophila. Proc. Natl. Acad. Sci. U. S. A. *109*, 6626–6631.
Rich, R.L., and Myszka, D.G. (2009). Extracting affinity constants from biosensor binding responses. In Label-Free Biosensors: Techniques and Applications, (Cambridge University Press), pp. 48–84.
Royer, L.A., Weigert, M., Günther, U., Maghelli, N., Jug, F., Sbalzarini, I.F., and Myers, E.W. (2015). ClearVolume: Open-source live 3D visualization for light-sheet microscopy. Nat. Methods *12*, 480–481.
Sanes, J.R., and Zipursky, S.L. (2020). Synaptic Specificity, Recognition Molecules, and Assembly of Neural Circuits. Cell *181*, 536–556.
Sarin, S., Zuniga-Sanchez, E., Kurmangaliyev, Y.Z., Cousins, H., Patel, M., Hernandez, J., Zhang, K.X., Samuel, M.A., Morey, M., Sanes, J.R., et al. (2018). Role for Wnt Signaling in Retinal Neuropil Development: Analysis via RNA-Seq and In Vivo Somatic CRISPR Mutagenesis. Neuron *98*, 109-126.e8.
Schindelin, J., Arganda-Carreras, I., Frise, E., Kaynig, V., Longair, M., Pietzsch, T., Preibisch, S., Rueden, C., Saalfeld, S., Schmid, B., et al. (2012). Fiji: An open-source platform for biological-image analysis. Nat. Methods *9*, 676–682.
Schwabe, T., Borycz, J.A., Meinertzhagen, I.A., and Clandinin, T.R. (2014). Differential Adhesion Determines the Organization of Synaptic Fascicles in the Drosophila Visual System. Curr. Biol. *24*, 1304–1313.
Sergeeva, A.P., Katsamba, P.S., Cosmanescu, F., Brewer, J.J., Ahlsen, G., Mannepalli, S., Shapiro, L., and Honig, B. (2020). DIP/Dpr interactions and the evolutionary design of specificity in protein families. Nat. Commun. *11*, 1–14.
Tan, L., Zhang, K.X., Pecot, M.Y., Nagarkar-Jaiswal, S., Lee, P.-T., Takemura, S., McEwen, J.M., Nern, A., Xu, S., Tadros, W., et al. (2015). Ig Superfamily Ligand and Receptor Pairs Expressed in Synaptic Partners in Drosophila. Cell *163*, 1756–1769.
Togane, Y., Ayukawa, R., Hara, Y., Akagawa, H., Iwabuchi, K., and Tsujimura, H. (2012). Spatio-temporal pattern of programmed cell death in the developing Drosophila optic lobe. Dev. Growth Differ. *54*, 503–518.
Trush, O., Liu, C., Han, X., Nakai, Y., Takayama, R., Murakawa, H., Carrillo, J.A., Takechi, H., Hakeda-Suzuki, S., Suzuki, T., et al. (2019). N-Cadherin Orchestrates Self-Organization of Neurons within a Columnar Unit in the Drosophila Medulla. J. Neurosci. *39*, 5861–5880.
Venkatasubramanian, L., Guo, Z., Xu, S., Tan, L., Xiao, Q., Nagarkar-Jaiswal, S., and Mann, R.S. (2019). Stereotyped terminal axon branching of leg motor neurons mediated by igsf proteins dip-α and dpr10. Elife *8*, e42692.

Xu, C., Theisen, E., Maloney, R., Peng, J., Santiago, I., Yapp, C., Werkhoven, Z., Rumbaut, E., Shum, B., Tarnogorska, D., et al. (2019). Control of Synaptic Specificity by Establishing a Relative Preference for Synaptic Partners. Neuron *103*, 1–13.
Xu, S., Xiao, Q., Cosmanescu, F., Sergeeva, A.P., Yoo, J., Lin, Y., Katsamba, P.S., Ahlsen, G., Kaufman, J., Linaval, N.T., et al. (2018). Interactions between the Ig-Superfamily Proteins DIP-α and Dpr6/10 Regulate Assembly of Neural Circuits. Neuron *100*, 1369-1384.e6.
Zhang, X., Koolhaas, W.H., and Schnorrer, F. (2014). A versatile two-step CRISPR- and RMCE-based strategy for efficient genome engineering in Drosophila. G3 Genes, Genomes, Genet. *4*, 2409–2418.
Zipursky, S.L., Venkatesh, T.R., Teplow, D.B., and Benzer, S. (1984). Neuronal development in the Drosophila retina: monoclonal antibodies as molecular probes. Cell *36*, 15–26.

Figure 1

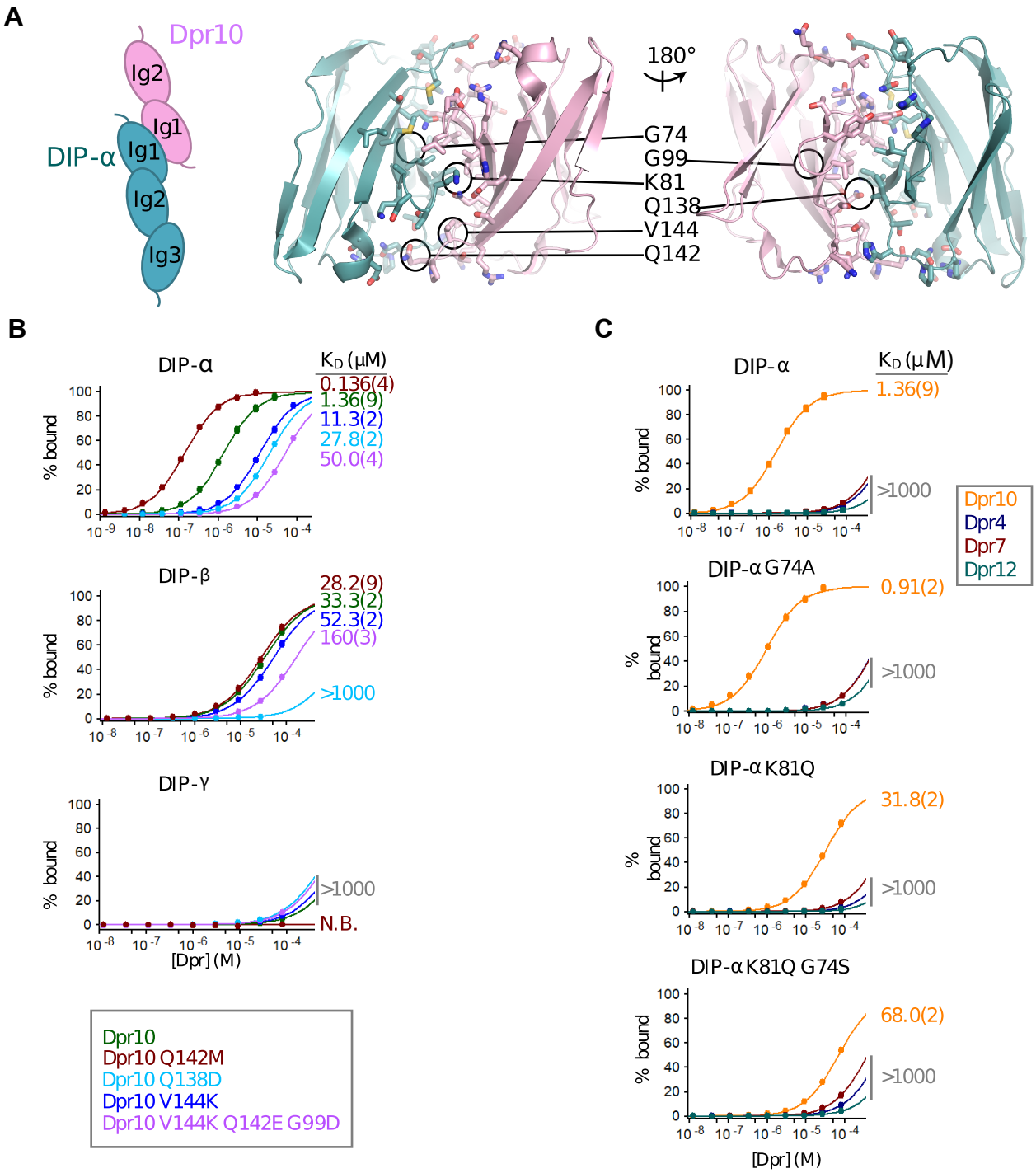
A
Dpr10
Ig2
Ig1
DIP-α
Ig1
Ig2
Ig3
180°
G74
G99
K81
Q138
V144
Q142
B
DIP-α
KD (μM)
0.136(4)
1.36(9)
11.3(2)
27.8(2)
50.0(4)
% bound
DIP-β
28.2(9)
33.3(2)
52.3(2)
160(3)
>1000
DIP-γ
>1000
N.B.
[Dpr] (M)
Dpr10
Dpr10 Q142M
Dpr10 Q138D
Dpr10 V144K
Dpr10 V144K Q142E G99D
C
DIP-α
KD (μM)
1.36(9)
>1000
Dpr10
Dpr4
Dpr7
Dpr12
DIP-α G74A
0.91(2)
>1000
DIP-α K81Q
31.8(2)
>1000
DIP-α K81Q G74S
68.0(2)
>1000
[Dpr] (M)

Figure 1. Biophysical analysis of interactions of DIP-α and Dpr10 mutants.

(A) Schematic representation of DIP-α/Dpr10 heterodimer formed between N-terminal Ig1 domains of DIP-α (in cyan) and Dpr10 (in pink), left, and the structure of the DIP-α/Dpr10 interface (PDBID: 6NRQ), right. Interfacial residues (within 6Å of the opposing protomer) are depicted as sticks and mutated positions are encircled and marked.

(B, C) Binding isotherms from SPR binding experiments. (B) Dpr10 and its mutants binding to DIP-α, DIP-β, and DIP-γ. (C) Dprs 10, 4, 7 and 12 binding to DIP-α and its mutants. The binding isotherms and the K_Ds are color-coded according to the legend shown to the right of each panel. K_Ds >1000 μM, describing multiple interactions are shown in grey. N.B. stands for no binding detected. The binding responses corresponding to the SPR experiments are shown in Fig. S1.

Figure 2

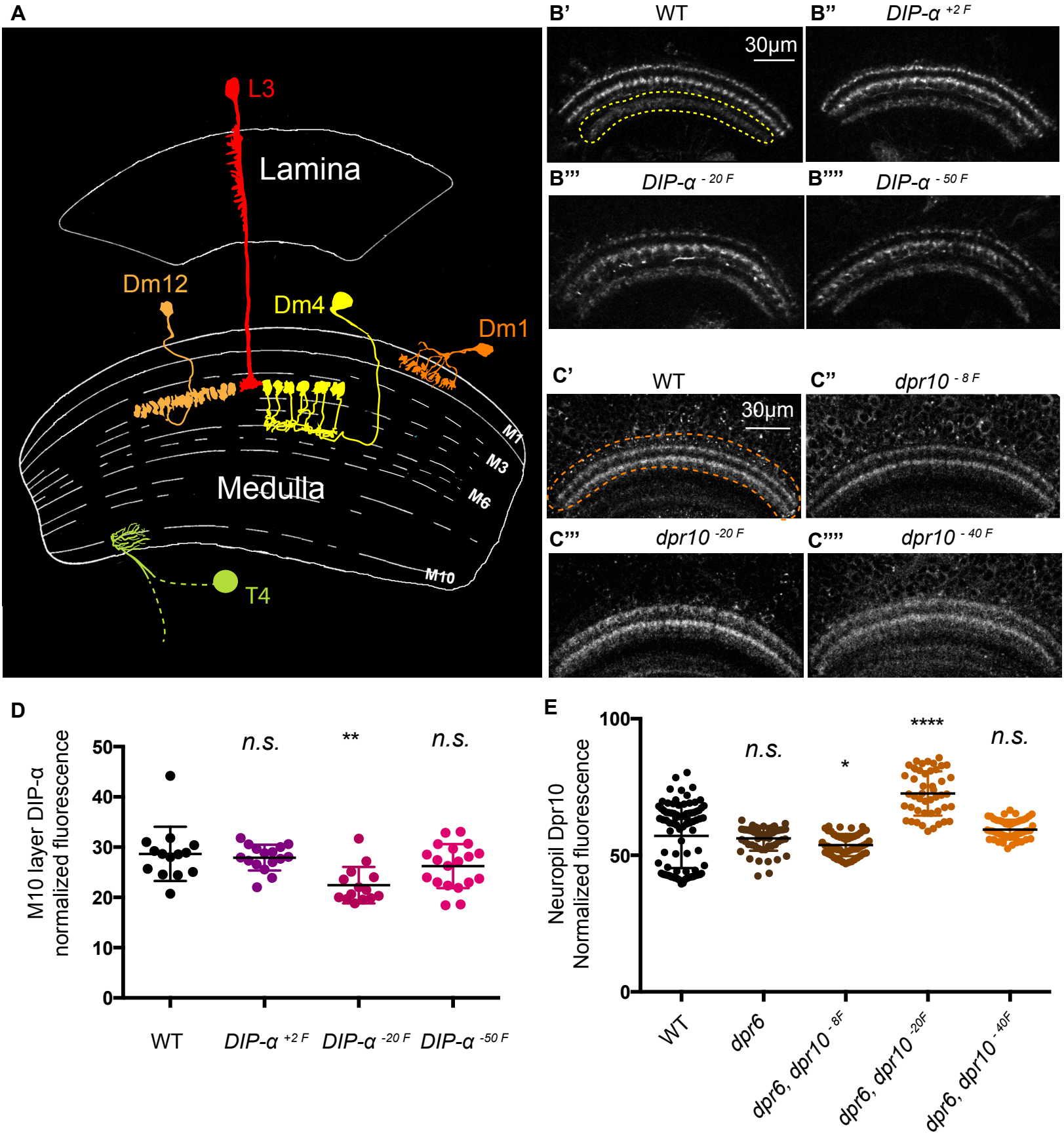
A
L3
Lamina
Dm12
Dm4
Dm1
Medulla
M1
M3
M6
M10
T4
B'
WT
30µm
B''
DIP-α +2 F
B'''
DIP-α - 20 F
B''''
DIP-α - 50 F
C'
WT
30µm
C''
dpr10 - 8 F
C'''
dpr10 -20 F
C''''
dpr10 - 40 F
D
M10 layer DIP-α
normalized fluorescence
50
40
30
20
10
0
n.s.
**
n.s.
WT
DIP-α +2 F
DIP-α -20 F
DIP-α -50 F
E
Neuropil Dpr10
Normalized fluorescence
100
50
0
n.s.
*
****
n.s.
WT
dpr6
dpr6, dpr10 - 8F
dpr6, dpr10 -20F
dpr6, dpr10 - 40F

Figure 2: DIP-α and Dpr10 mutant proteins are expressed in wild-type patterns and at comparable levels.

(A) Schematic of the lamina and medulla neuropil areas of adult *Drosophila* OL. The cell types studied in this paper are indicated.

(B) Anti-DIP-α antibody staining of medulla region in wild type and *DIP-α* affinity mutants at 48h APF. Genotype in B, B'', B''' and B'''', wild-type, *DIP-α*$^{+2F}$, *DIP-α*$^{-20F}$, *DIP-α*$^{-50F}$. Scale bar: 30μm.

(C) Anti-Dpr10 antibody staining of medulla region in wild type and *dpr10* affinity mutants at 48h APF. Genotype in C, C', C'', C''', wild-type, *dpr10*$^{-8F}$, *dpr10*$^{-20F}$, *dpr10*$^{-40F}$. Scale bar: 30 μm.

(D) Quantification of anti-DIP-α fluorescence signal intensity of the most proximal medulla layer (M10) at 48h APF (yellow dotted circle in b') in wild type and *DIP-α* affinity mutants. (*p* value calculated against wild-type. ***p*=0.0014. unpaired t test.)

(E) Quantification of anti-Dpr10 fluorescence signal intensity of the two Dpr10 expressing neuropil layers (orange dotted circle in c') in wild type and *dpr10* affinity mutants. (p value calculated against wild-type. **p*=0.0481. *****p*<0.0001. unpaired t test.) For d and e, samples were mounted dorsal up. For each sample, 15 slices of confocal images were taken starting from 50 μm away from the surface, at 5 μm step size. Each slice was analyzed separately for fluorescence intensity in ROI. Fluorescence intensity was normalized against background signal.

Figure 3

A

Dm12> myrtdTomato

WT

20µm

Dm12-myrtdTomato BRP

A'

M3

M8

B

Dm12> myrtdTomato

DIP-α -

B'

M3

M8

Dm12>myrtdTomato; DIP-α -20F

Dm12>myrtdTomato; DIP-α -50F

Dm12>myrtdTomato; DIP-α -20F; dpr6null

Dm12>myrtdTomato; DIP-α -50F; dpr6null

Dm12>myrtdTomato; DIP-αnull

C

10µm

D

E

F

G

Dm12>myrtdTomato; dpr6null

Dm12>myrtdTomato; dpr6null ,dpr10 -8F

Dm12>myrtdTomato; dpr6null ,dpr10 -20F

Dm12>myrtdTomato; dpr6null ,dpr10 -40F

Dm12>myrtdTomato; dpr6null,dpr10null

H

I

J

K

L

M

Dm12 mistargeted (#)

60

40

20

0

**

****

****

****

****

***

****

****

****

DIP-α WT -20F -50F -20F -50F - WT WT WT WT WT

Dpr10 WT WT WT WT WT WT WT -8F -20F -40F -

Dpr6 WT WT WT - - WT - - - - -

N

Dm12 cell loss (#)

40

20

0

-20

-40

n.s.

****

**

****

****

n.s.

n.s.

**

***

DIP-α WT -20F -50F -20F -50F - WT WT WT WT WT

Dpr10 WT WT WT WT WT WT WT -8F -20F -40F -

Dpr6 WT WT WT - - WT - - - - -

O

DIP-α/Dpr10 Q142M +10F

DIP-α/Dpr10 WT

DIP-α/Dpr10 V144K -8F

DIP-α/Dpr10 Q138D -20F

DIP-α/Dpr10 G99D Q142E V144K -40F

(Affinity fold change)

Strong Binding

0.14

1.4

11.3

27.8

50.0

Weak binding

K_{Dr} µM

0.9

31.8

68.0

+2F DIP-αG74A/Dpr10

DIP-αK81Q/Dpr10 -20F

DIP-αK81Q G74S /Dpr10 -50F

Dm12

Wild Type

Targeting Threshold

Survival Threshold

Null

Figure 3: *DIP-α* affinity mutants display different thresholds for Dm12 synaptic targeting and for cell survival.

(A-D) Dm12 neurons in wild type and *DIP-α*^{null} adult medulla. White, Dm12 neurons labeled with Dm12-LexA>LexAop-myrtdTomato; Green, anti-Bruchpilot staining showing medulla layers. Each panel is a maximum intensity projection (MIP) of a ~10 micron *Z*-stack, at 0.18 micron slice interval, of the entire medulla neuropil. Black dotted line: M3 layer; yellow dotted line: M8 layer; yellow arrow: axons of mistargeted Dm12 neuron from M3 to M8. Scale bar: 20 μm.

(C-L) Dm12 neurons in *DIP-α* or *dpr10* affinity mutants. Genotypes as indicated. Each panel is a MIP of a ~10 micron *Z*-stack, with 0.18 micron slice interval. Images show representative windows of the entire medulla. Yellow arrow: axons of mistargeted Dm12 neuron. Scale bar: 10 μm.

(M) Number of Dm12 neurons that mistarget to the M8 layer in wild-type and *DIP-α* mutant OLs as indicated. The number of mistargeted Dm12 neurons is quantified as the number of Dm12 axons projecting from M3 to M8 (yellow arrows A-L). (*p* value was calculated against wild-type for flies carrying *DIP-α* mutation, and against *dpr6*^{null} for flies carrying *dpr6*^{null} *dpr10* mutations. ***p*<0.01. ****p*<0.001. *****p*<0.0001. unpaired t test.)

(N) Number of missing Dm12 cells in wild-type and *DIP-α* affinity mutant OLs as indicated. Total number of missing Dm12 neurons was quantified as (average wild type Dm12 neuron number) – (Dm12 neuron number in each OL). Dm12 neuron number is quantified as the number of Dm12 cell bodies in one OL. (*p* value was calculated against wild-type for flies carrying *DIP-α* mutation, and

against *dpr6*^{null} for flies carrying *dpr6*^{null} *dpr10* mutations. ***p*<0.01; ****p*<0.001. unpaired *t*-test.)

(O) K_Ds of *DIP-α* and *dpr10* affinity mutant protein binding to the wildtype partner are marked on the scaled line. Dm12 targeting and cell loss thresholds are marked at the position where a penetrance of ~50% of the null penetrance is observed.

Figure 4

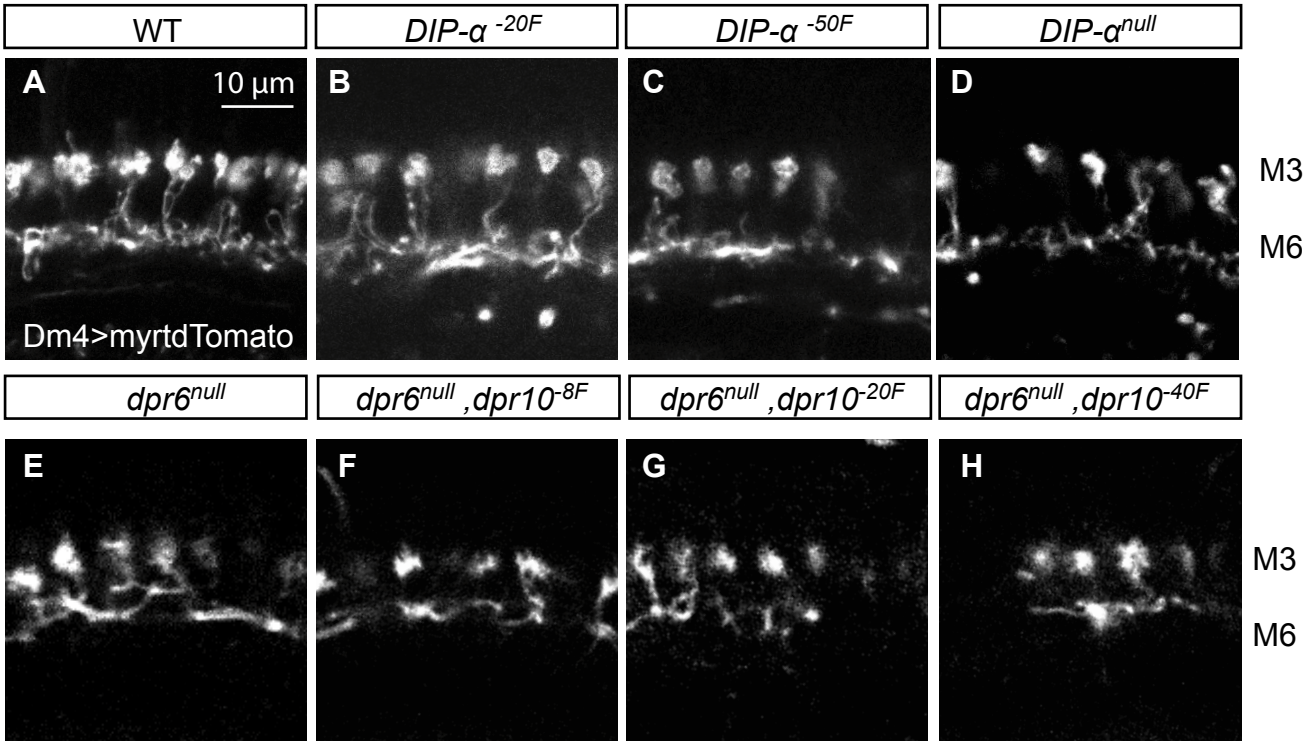
WT
DIP-α -20F
DIP-α -50F
DIP-α null
A
10 µm
B
C
D
Dm4>myrtdTomato
M3
M6
dpr6 null
dpr6 null ,dpr10 -8F
dpr6 null ,dpr10 -20F
dpr6 null ,dpr10 -40F
E
F
G
H
M3
M6

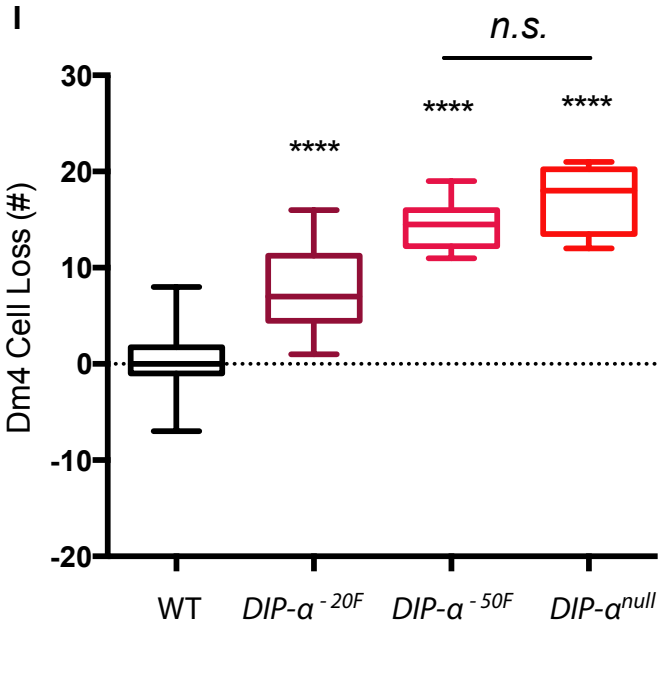
I
n.s.
****
****
****
30
20
10
0
-10
-20
Dm4 Cell Loss (#)
WT
DIP-α -20F
DIP-α -50F
DIP-α null

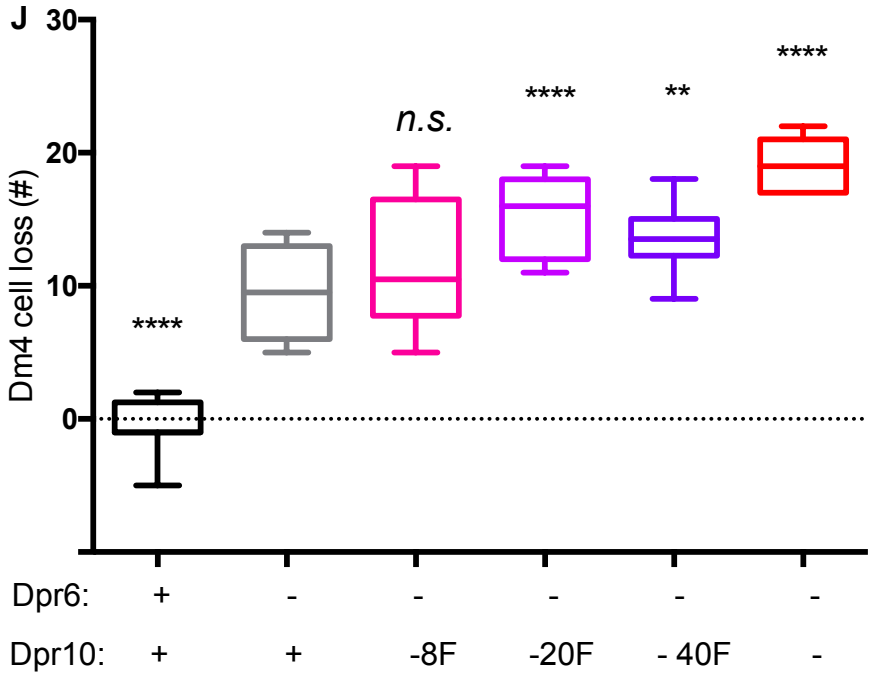
J
30
20
10
0
Dm4 cell loss (#)
****
n.s.
****
**
****
Dpr6: + - - - - -
Dpr10: + + -8F -20F - 40F -

Figure 4: Dm4 neurons show graded cell loss as DIP-α::Dpr10 affinity is reduced.

(A-H) Dm4 neurons are labeled by Dm4-LexA>LexAop-myrtdTomato. Each panel is a representative window of a single slice confocal image of the medulla. Genotypes as indicated. Scale bar: 10 μm.

(I) Number of Dm4 cells lost in *DIP-α* mutants. (*p* value calculated against wildtype. ****p<0.0001. unpaired t test.)

(J) Numbers of Dm4 cells lost in *dpr6 dpr10* mutants. (*p* value calculated against $dpr6^{null}$. **p<0.01. ****p<0.0001. unpaired *t*-test.)

Figure 5

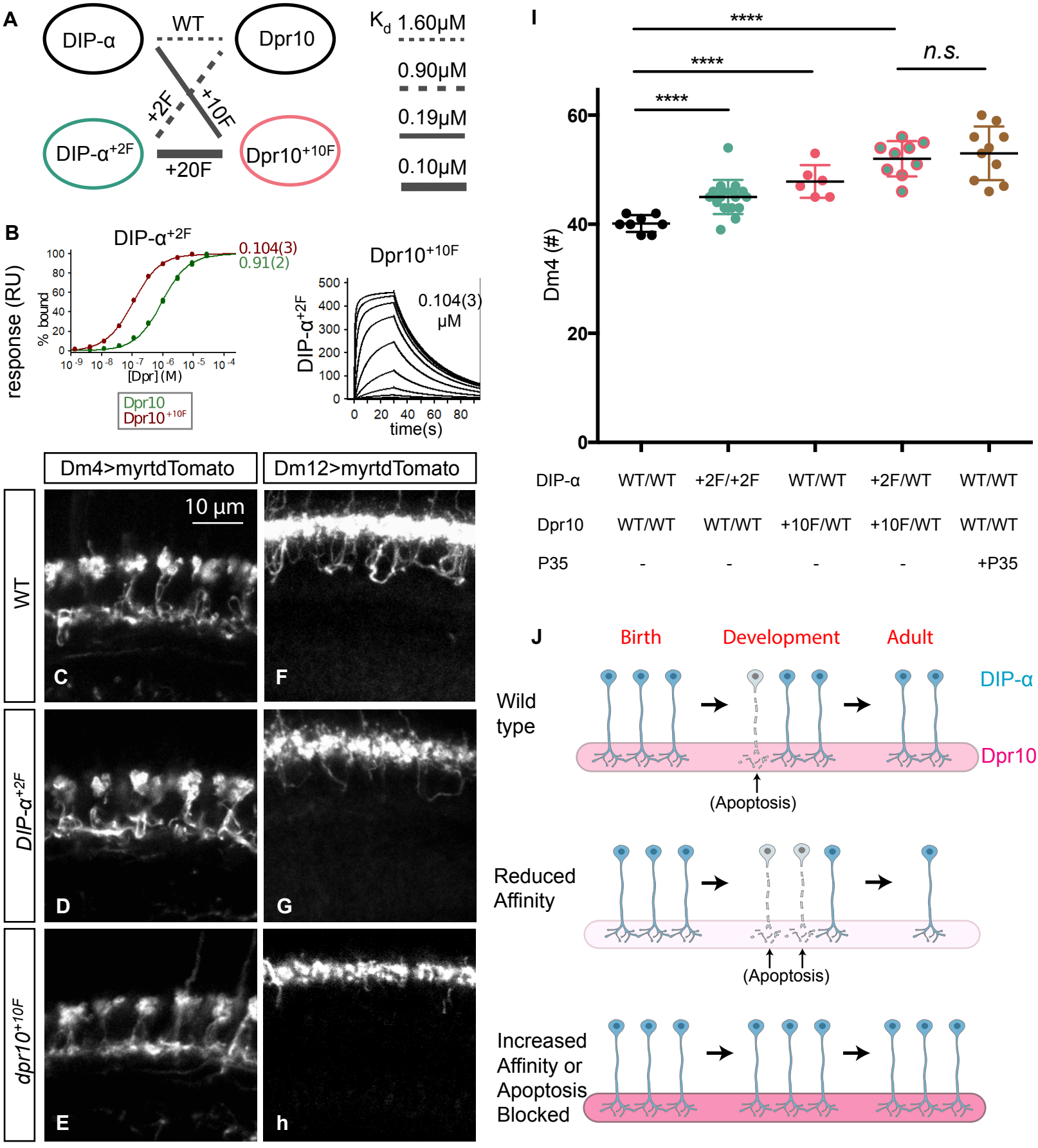
A
DIP-α
WT
Dpr10
+2F
+10F
DIP-α+2F
+20F
Dpr10+10F
Kd 1.60μM
0.90μM
0.19μM
0.10μM
B
DIP-α+2F
0.104(3)
0.91(2)
% bound
[Dpr] (M)
Dpr10
Dpr10+10F
Dpr10+10F
DIP-α+2F
0.104(3) μM
time(s)
response (RU)
Dm4>myrtdTomato
Dm12>myrtdTomato
10 μm
WT
DIP-α+2F
dpr10+10F
C
F
D
G
E
h
I
****
****
****
n.s.
Dm4 (#)
DIP-α WT/WT +2F/+2F WT/WT +2F/WT WT/WT
Dpr10 WT/WT WT/WT +10F/WT +10F/WT WT/WT
P35 - - - - +P35
J
Birth
Development
Adult
Wild type
DIP-α
Dpr10
(Apoptosis)
Reduced Affinity
(Apoptosis)
Increased Affinity or Apoptosis Blocked

Figure 5: Increasing DIP-α::Dpr10 affinity prevents the normal culling of Dm4 neurons.

(A) Diagram of binding affinities among wild-type and increased affinity DIP-α and Dpr10 mutant proteins (DIP-α^{+2F} and $Dpr10^{+10F}$).

(B) Left: Dpr10 and $Dpr10^{+10F}$ binding to DIP-α^{+2F}. The binding isotherms and the K_Ds are color-coded according to the legend shown to the bottom of the panel. Right: The binding responses between $Dpr10^{+10F}$ and DIP-α^{+2F} corresponding to the SPR experiments on the left.

(C-H) Dm4 (c-e) or Dm12 (f-h) neurons in flies expressing wild type or affinity increased DIP-α or Dpr10 proteins. Genotypes as indicated. Dm4 neurons are labeld with Dm4-LexA>LexAop-myrtdTomato. Dm12 neurons are labeled with Dm12-LexA>LexAop-myrtdTomato. Each panel is a representative window of a single slice confocal image of the medulla. Scale bar, 10 μm.

(I) Numbers of Dm4 neurons in wild type, affinity increased, or apoptosis blocked flies. Genotypes as indicated. (*p* value calculated against wildtype. ****$p<0.0001$. unpaired t test.)

(J) Schematic representation of Dm4 development in wildtype, affinity reduced mutant, affinity increased mutant, or apoptosis blocked flies. Saturation of the pink bar represents affinity between DIP-α and Dpr10. Grey cells represent apoptotic cells.

Figure 6

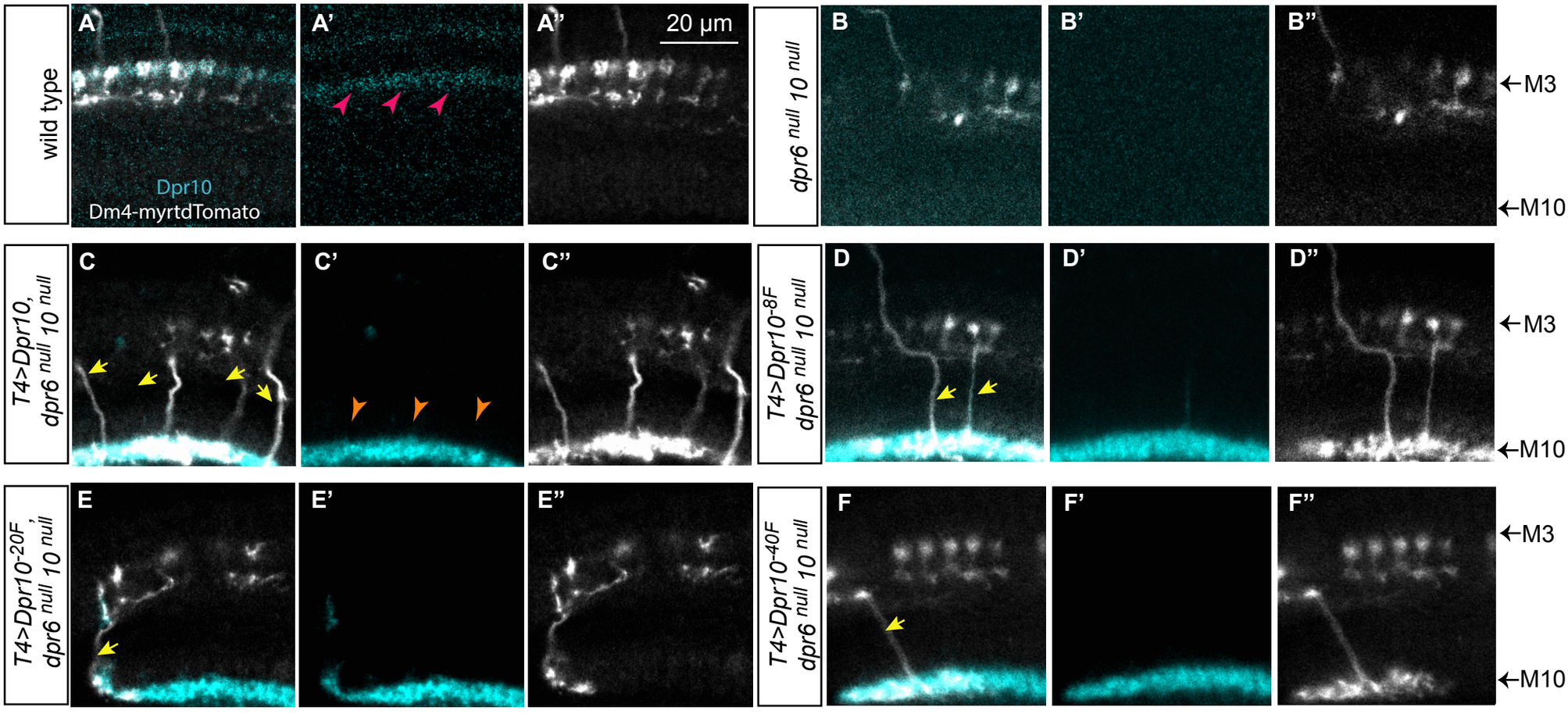
wild type
A
A'
A''
20 µm
Dpr10
Dm4-myrtdTomato
dpr6 null 10 null
B
B'
B''
←M3
←M10
T4>Dpr10, dpr6 null 10 null
C
C'
C''
T4>Dpr10-8F dpr6 null 10 null
D
D'
D''
T4>Dpr10-20F, dpr6 null 10 null
E
E'
E''
T4>Dpr10-40F dpr6 null 10 null
F
F'
F''

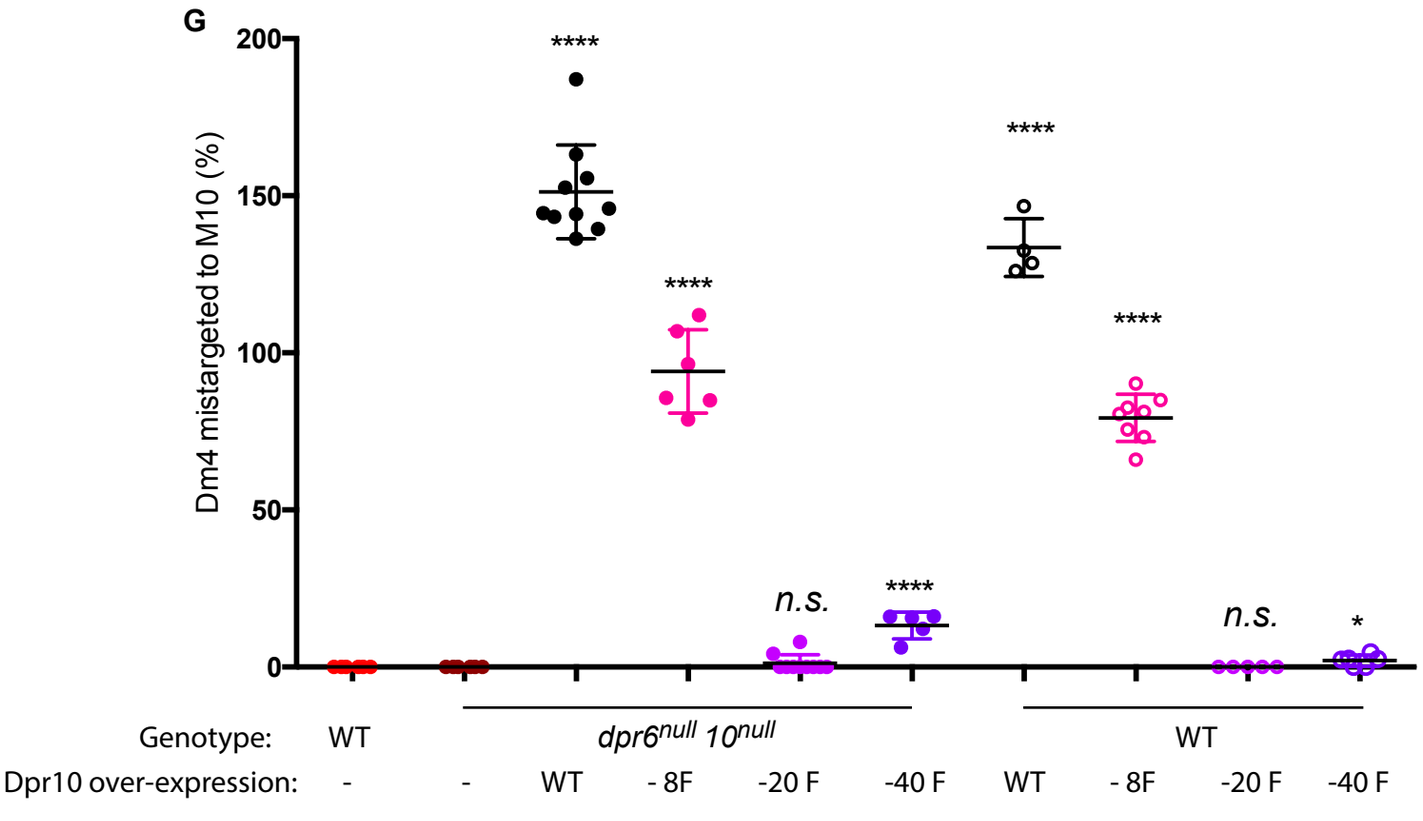
G
Dm4 mistargeted to M10 (%)
200
150
100
50
0
****
****
****
****
n.s.
****
n.s.
*
Genotype:
WT
dpr6null 10null
WT
Dpr10 over-expression:
-
-
WT
- 8F
-20 F
-40 F
WT
- 8F
-20 F
-40 F

Figure 6: An affinity threshold for induction of mistargeting by ectopic Dpr10.

(A-F) Dm4 neurons at 48h APF. a, wild type; b, *dpr6*^{null} *dpr10*^{null}; c-f, misexpression of wild type or mutant Dpr10 proteins in M10 layer by T4-Gal4, in *dpr6*^{null}, *dpr10*^{null} OLs. Misexpressed proteins are as indicated. The images show one representative area of a single confocal slice of the medulla. White, Dm4 (labeled with Dm4-LexA>LexAop-myrtdTomato); cyan: Dpr10. Scale bar: 20 μm. (G) Graph summarizings panel a-f, plus data showing over-expression of Dpr10 wild-type or mutant proteins in the wild-type background. In both genetic backgrounds, Dpr10^{-8F} induces mistargeting, but Dpr10^{-20F} and Dpr10^{-40F} do not. (*p* value calculated against wild-type. **p*=0.0188. ****p<0.0001. unpaired *t*-test).

Figure 7

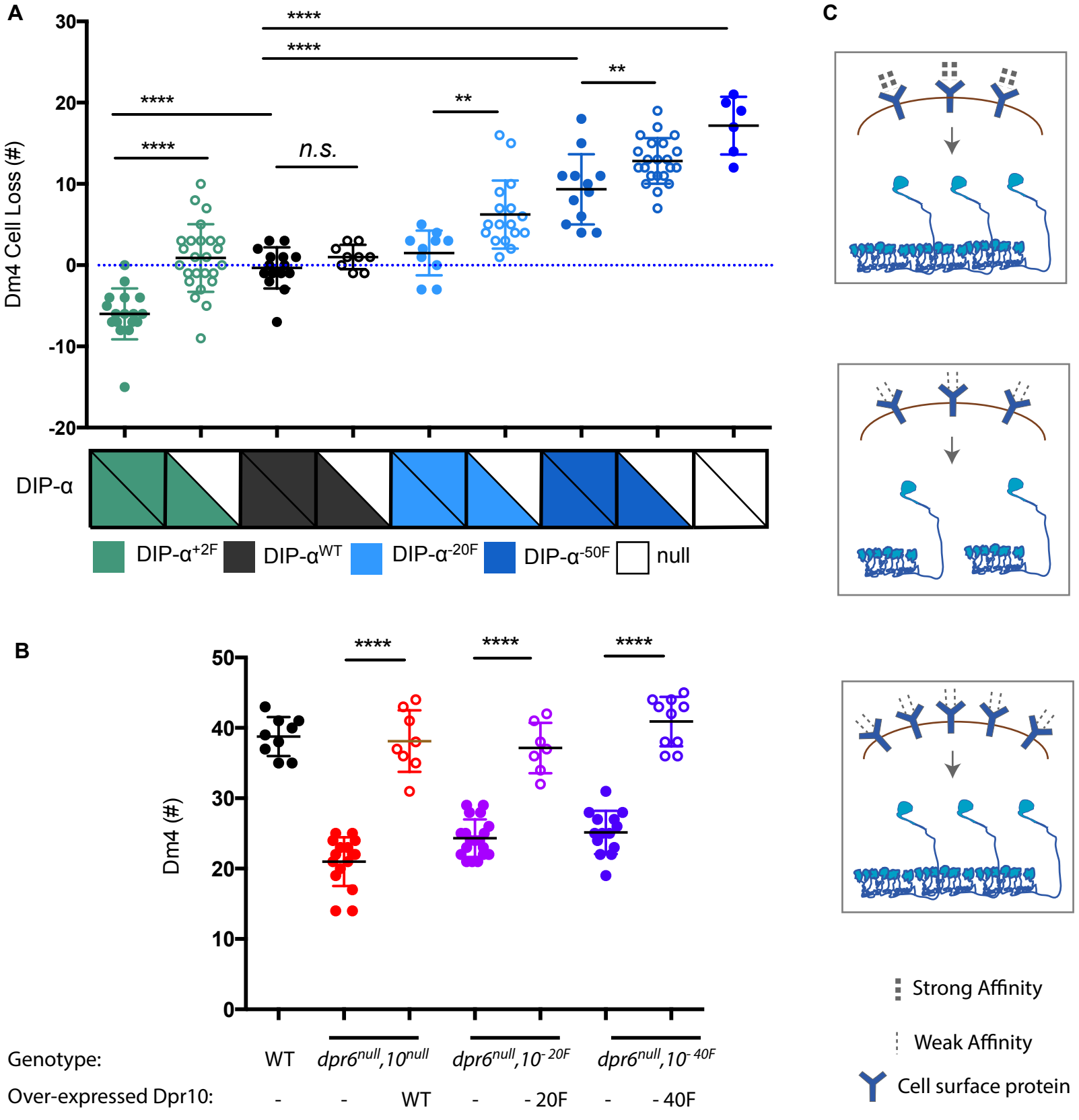
A
Dm4 Cell Loss (#)
30
20
10
0
-10
-20
****
****
****
n.s.
**
**
DIP-α
DIP-α+2F
DIP-αWT
DIP-α-20F
DIP-α-50F
null
B
Dm4 (#)
50
40
30
20
10
0
****
****
****
Genotype:
WT
dpr6null,10null
dpr6null,10-20F
dpr6null,10-40F
Over-expressed Dpr10:
-
-
WT
-
- 20F
-
- 40F
C
Strong Affinity
Weak Affinity
Cell surface protein

Figure 7. Cell surface avidity is a key parameter controlling circuit assembly.

(A) Numbers of Dm4 cells lost in flies expressing one or two copies of wild type or mutant DIP-α proteins. Genotypes are as indicated. ***p*=0.0039 (*DIP-α*$^{-20F}$ group), ***p*=0.0075 (*DIP-α*$^{-50F}$ group). *****p*<0.0001, unpaired *t*-test.

(B) Numbers of Dm4 neurons in animals overexpressing Dpr10^{-20F} or Dpr10^{-40F} in L3, In the indicated backgrounds. (*****p*<0.0001. unpaired t test.)

(C) Schematic diagram of the effects of individual protein-protein binding affinity and protein copy number on cell survival. When cells express a reduced affinity cell surface protein, increased cell death is observed. Reduced affinity can be compensated by expressing more copies of the same protein.

SUPPLEMENTAL FIGURES, TABLE, AND FIGURE LEGEND:

Affinity Requirements For Control Of Synaptic Targeting And Neuronal Cell Survival By Heterophilic IgSF Cell Adhesion Molecules

Shuwa Xu[1]*, Alina P Sergeeva[2], Phinikoula S. Katsamba[3], Seetha Mannepalli[3], Fabiana Bahna[3], Jude Bimela[3], S. L Zipursky[4], Lawrence Shapiro[3,5], Barry Honig[2,3,5,6], Kai Zinn[1]*

[1]California Institute of Technology, Biology and Biological Engineering, Pasadena, CA,
[2]Department of Systems Biology, Columbia University Medical Center, New York, NY 10032, USA
[3]Zuckerman Mind Brain and Behavior Institute, Columbia University, New York, NY 10027, USA
[4]Department of Biological Chemistry, HHMI, David Geffen School of Medicine, University of California, Los Angeles, Los Angeles, CA 90095, USA
[5]Department of Biochemistry and Molecular Biophysics, Columbia University, New York, NY 10032, USA
[6]Department of Medicine, Columbia University, New York, NY 10032, USA

*Corresponding authors:
Shuwa Xu (shuwaxu@caltech.edu), Kai Zinn (zinnk@caltech.edu).

Table S1 (AUC data for homodimer mutants)

Protein-protein interaction	**K_D (homophilic), µM**
DIP-α/DIP-α WT	23.9 ± 0.0[a]
DIP-α G74A /DIP-α G74A	50.0 ± 0.6[b]
DIP-α K81Q /DIP-α K81Q	19.7 ± 1.9[b]
DIP-α K81Q G74S /DIP-α K81Q G74S	46.3 ± 5.7[b]

[a] Published in Cosmanescu et al (2018)
[b] Published in Sergeeva et al (2020)

Figure S1

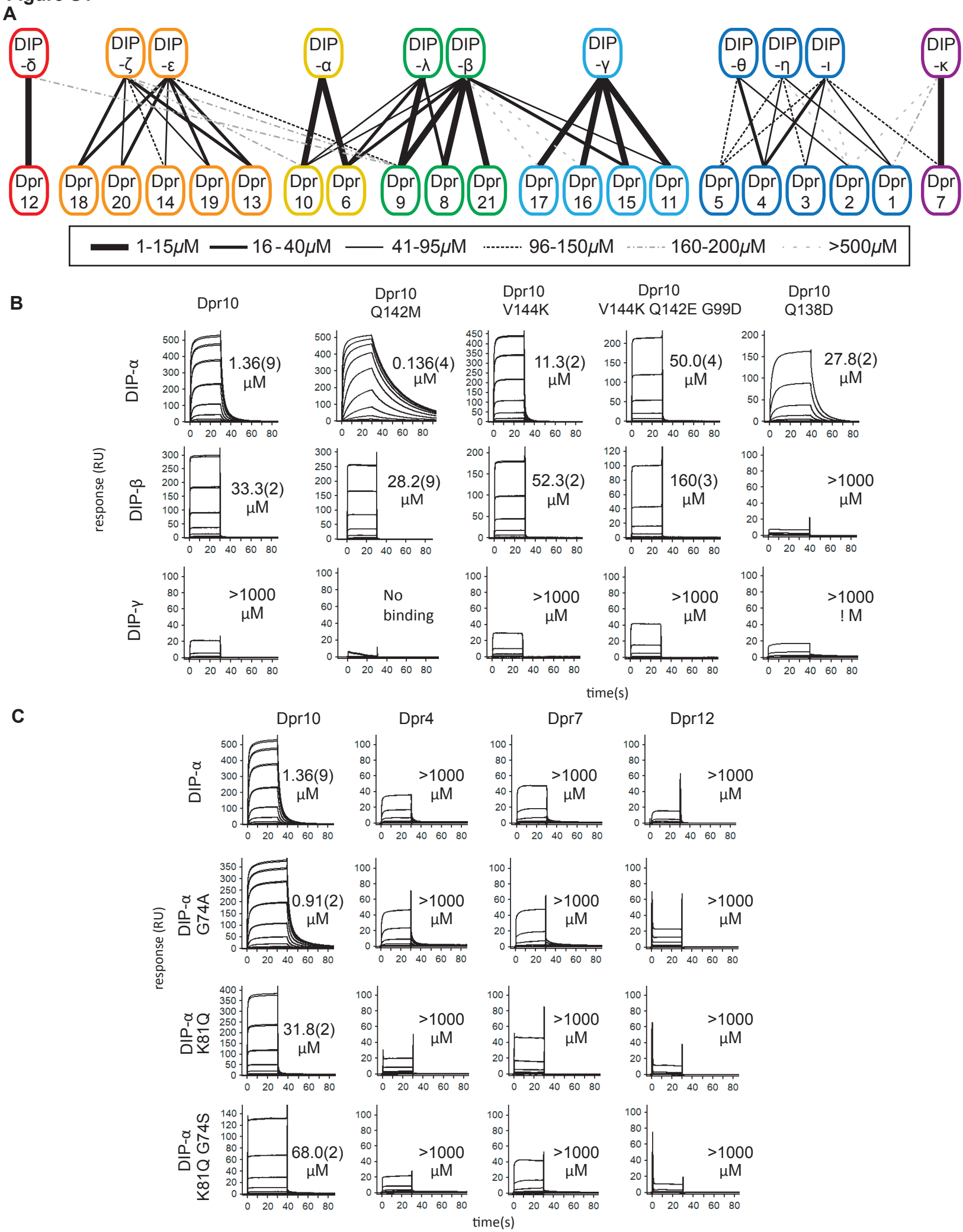
A
DIP -δ
DIP -ζ
DIP -ε
DIP -α
DIP -λ
DIP -β
DIP -γ
DIP -θ
DIP -η
DIP -ι
DIP -κ
Dpr 12
Dpr 18
Dpr 20
Dpr 14
Dpr 19
Dpr 13
Dpr 10
Dpr 6
Dpr 9
Dpr 8
Dpr 21
Dpr 17
Dpr 16
Dpr 15
Dpr 11
Dpr 5
Dpr 4
Dpr 3
Dpr 2
Dpr 1
Dpr 7
1-15μM
16-40μM
41-95μM
96-150μM
160-200μM
>500μM
B
Dpr10
Dpr10 Q142M
Dpr10 V144K
Dpr10 V144K Q142E G99D
Dpr10 Q138D
DIP-α
DIP-β
DIP-γ
response (RU)
1.36(9) μM
0.136(4) μM
11.3(2) μM
50.0(4) μM
27.8(2) μM
33.3(2) μM
28.2(9) μM
52.3(2) μM
160(3) μM
>1000 μM
>1000 μM
No binding
>1000 μM
>1000 μM
>1000 ! M
time(s)
C
Dpr10
Dpr4
Dpr7
Dpr12
DIP-α
DIP-α G74A
DIP-α K81Q
DIP-α K81Q G74S
response (RU)
1.36(9) μM
>1000 μM
>1000 μM
>1000 μM
0.91(2) μM
>1000 μM
>1000 μM
>1000 μM
31.8(2) μM
>1000 μM
>1000 μM
>1000 μM
68.0(2) μM
>1000 μM
>1000 μM
>1000 μM
time(s)

Figure S1. SPR binding experiments for Dpr10 and DIP-α mutants.

(A) Schematic of DIP/Dpr-ome, modified from Sergeeva *et.al* 2020.
(B) SPR responses for Dpr 10 and its mutants Q142M, V144K, V144K Q142E G99D and Q138D, binding over surfaces immobilized with DIP-α (first row), DIP-β (second row), and DIP-γ (third row).
(C) SPR responses for Dprs 10, 4, 7 and 12 binding over surfaces immobilized with DIP-α (first row), DIP-α G74A (second row), DIP-α K81Q (third row) and DIP-α K81Q G74S (fourth row). The isotherms describing the SPR data are shown in Fig. 1b-c. The Dpr concentrations used in each binding assay are listed in the method details section for SPR experiments.

Figure S2

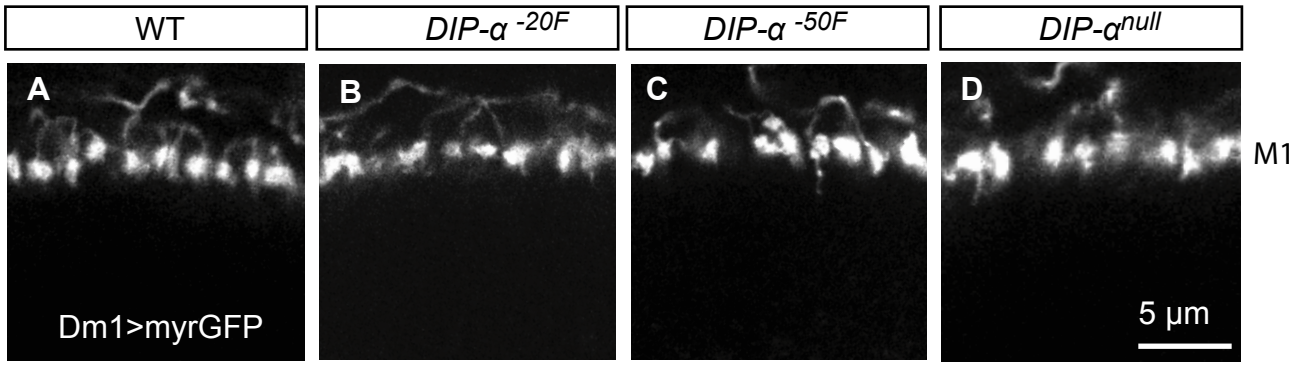
WT
DIP-α -20F
DIP-α -50F
DIP-αnull
A
B
C
D
Dm1>myrGFP
5 µm
M1

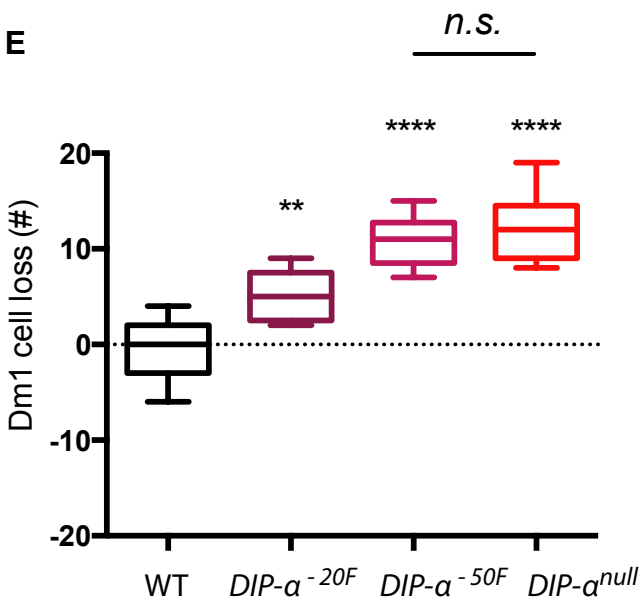
E
n.s.
****
****
**
20
10
0
-10
-20
Dm1 cell loss (#)
WT
DIP-α -20F
DIP-α -50F
DIP-αnull

Figure S2: Dm1 neurons show graded cell loss with reduced DIP-α::Dpr10 affinity in *DIP-α* mutants.
(A-D) Images are showing one representative area of a single confocal slice of the medulla. Dm1 neurons were labeled by Dm1-Gal4;UAS-myrGFP. Genotypes as indicated. Scale bar: 5 μm.
(E) Graph summarizing panel a-d, showing number of Dm1 cell loss in different *DIP-α* genotypes. (p value calculated against wild type. **p=0.0030. ****p<0.0001. unpaired t test.)

Figure S3

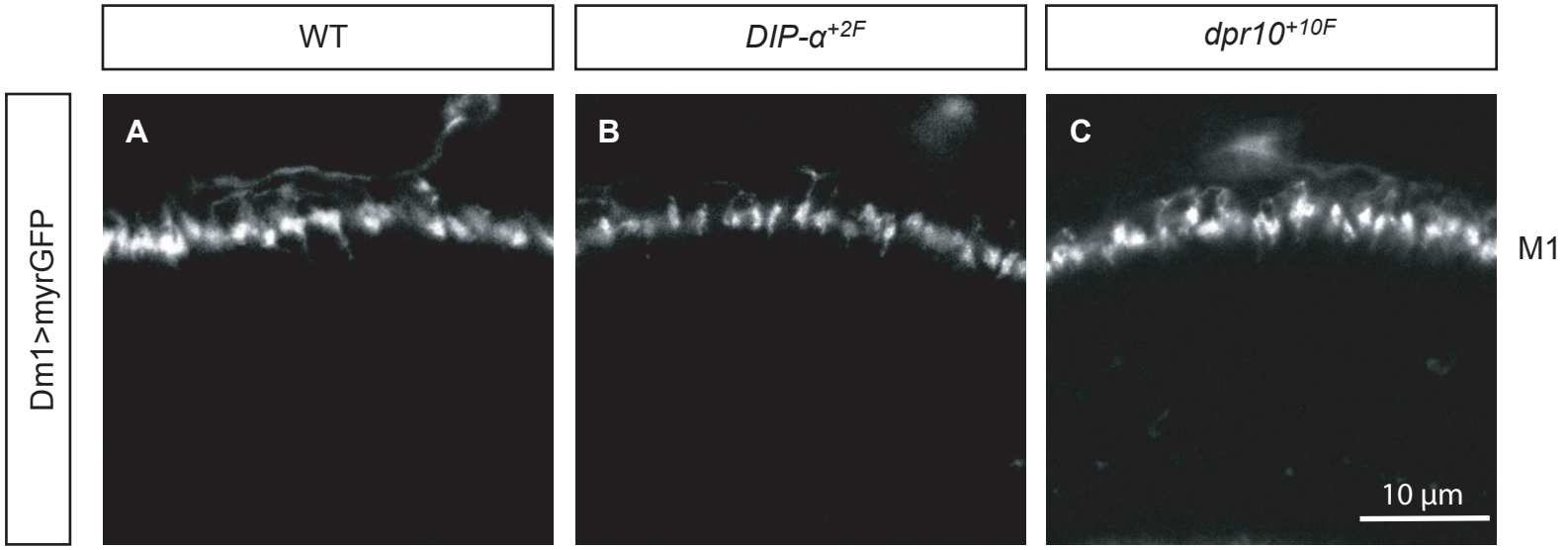

Figure S3: Dm1 neurons show normal morphology and targeting in mutants that increase DIP-α::Dpr10 affinity.
Dm1 neurons were labeled by Dm1-Gal4;UAS-myrGFP. Each image shows a representative area of a single confocal slice of the medulla. Genotypes as indicated. Scale bar: 10 μm.

Figure S4

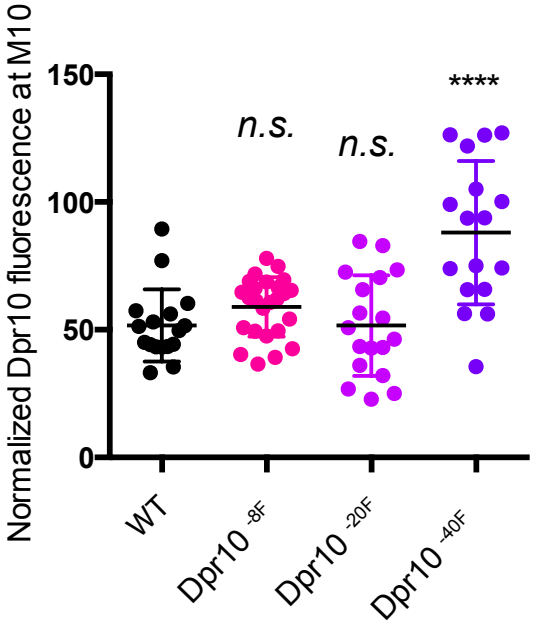
Normalized Dpr10 fluorescence at M10
150
100
50
0
n.s.
n.s.
****
WT
Dpr10 -8F
Dpr10 -20F
Dpr10 -40F

Figure S4: Normalized fluorescence intensity of anti-Dpr10 signals from over-expressed wild type or mutant Dpr10 proteins in M10 layer.
(p value calculated against wild-type. ****p<0.0001. unpaired t test).

Figure S5

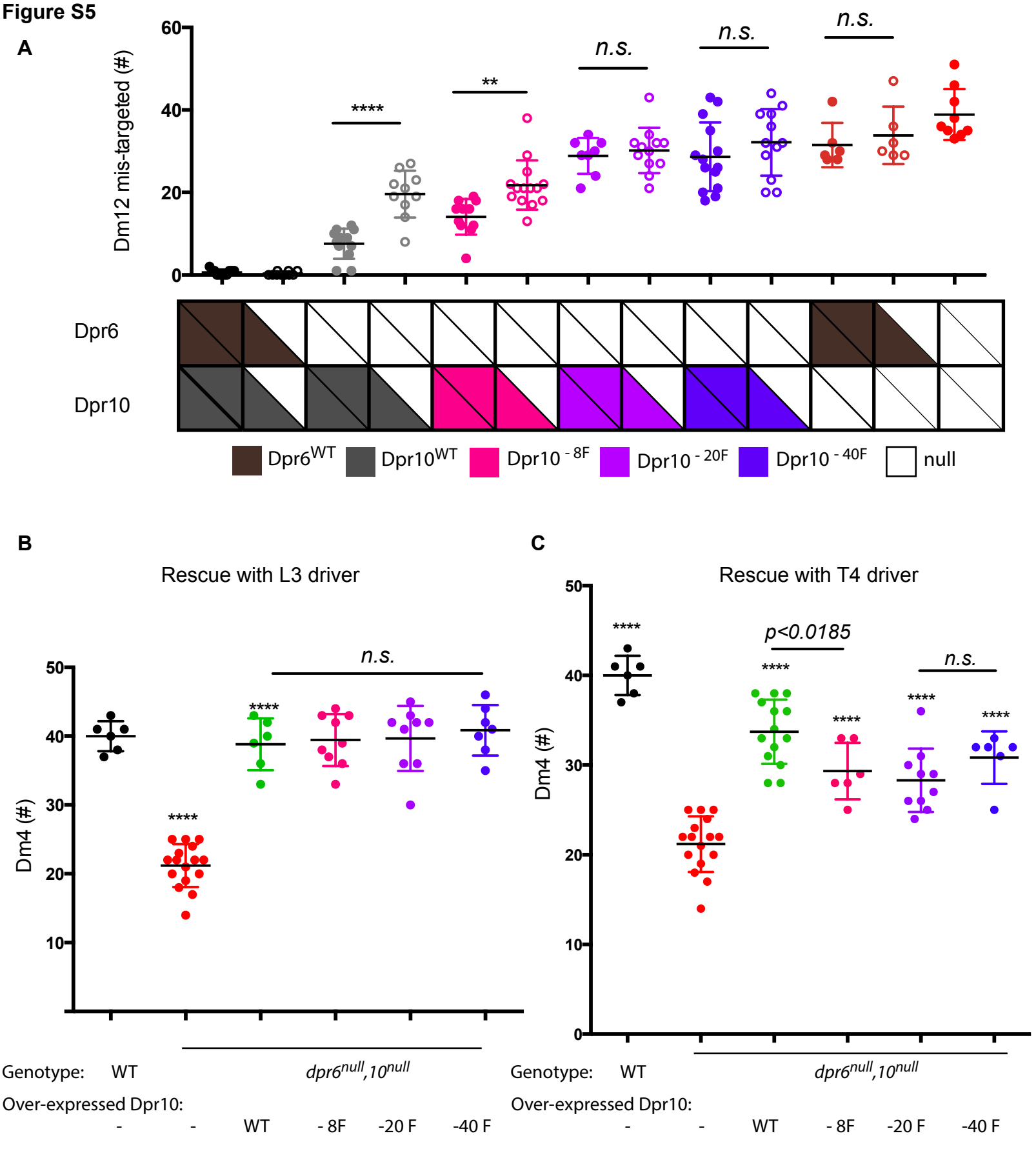
A
Dm12 mis-targeted (#)
60
40
20
0
****
**
n.s.
n.s.
n.s.
Dpr6
Dpr10
Dpr6WT
Dpr10WT
Dpr10 - 8F
Dpr10 - 20F
Dpr10 - 40F
null
B
Rescue with L3 driver
Dm4 (#)
50
40
30
20
10
****
n.s.
Genotype: WT dpr6null,10null
Over-expressed Dpr10:
- - WT - 8F -20 F -40 F
C
Rescue with T4 driver
Dm4 (#)
50
40
30
20
10
0
****
p<0.0185
****
n.s.
****
****
****
Genotype: WT dpr6null,10null
Over-expressed Dpr10:
- - WT - 8F -20 F -40 F

Figure S5: Protein expression levels contribute to cell surface avidity.
(A) Number of Dm12 neurons that mistarget in flies expressing one or two copies of wild type or mutant Dpr6 or Dpr10 protein. Genotypes are as indicated.
(**p=0.0016. ****p<0.0001. unpaired t test.)
(B) Number of Dm4 neurons in fly OL overexpressing $Dpr10^{WT}$, $Dpr10^{-8F}$, $Dpr10^{-20F}$, or $Dpr10^{-40F}$ in L3 in *dpr6*$^{-}$ *dpr10*$^{-}$ double null flies. (p value calculated against *dpr6*$^{-}$ *dpr10*$^{-}$. ****p<0.0001. unpaired t test.)
(C) UAS-$Dpr10^{-8F}$, UAS-$Dpr10^{-20F}$, UAS-$Dpr10^{-40F}$, or UAS-$Dpr10^{WT}$ are expressed by T4-Gal4 that drives transgene expression at early pupal development stages before16h APF. (p value calculated against *dpr6*$^{-}$ *dpr10*$^{-}$ double null. ****p<0.0001. unpaired t test.)

Supplemental File 1: Genotypes of flies used in this study

Figure 2	
2b'	wild type
2b''	*DIP-α*$^{+2F}$
2b''''	*DIP-α*$^{-20F}$
2b''''	*DIP-α*$^{-50F}$
2c'	wild type
2c''	*Dpr10*$^{-8F}$
2c'''	*Dpr10*$^{-20F}$
2c''''	*Dpr10*$^{-40F}$
2d (from left to right)	wild type *DIP-α*$^{+2F}$ *DIP-α*$^{-20F}$ *DIP-α*$^{-50F}$
2e (from left to right)	wild type *dpr6*^{null} *dpr6*^{null}, *dpr10*$^{-8F}$ *dpr6*^{null}, *dpr10*$^{-20F}$ *dpr6*^{null}, *dpr10*$^{-40F}$
Figure 3	
3a, 3a'	w'; 47G08LexA-LexAop-myrtdTomato/+; +/+
3b, 3b'	*DIP-α*^{null}/*DIP-α*^{null}, 47G08LexA-LexAop-myrtdTomato/+; +/+
3c	*DIP-α*$^{-20F}$/*DIP-α*^{null}, 47G08LexA-LexAop-myrtdTomato/+; +/+
3d	*DIP-α*$^{-50F}$/*DIP-α*^{null}, 47G08LexA-LexAop-myrtdTomato/+; +/+
3e	*DIP-α*$^{-20F}$/*DIP-α*^{null}, 47G08LexA-LexAop-myrtdTomato/+; *dpr6*^{null}/*dpr6*^{null}
3f	*DIP-α*$^{-50F}$/*DIP-α*^{null}, 47G08LexA-LexAop-myrtdTomato/+; *dpr6*^{null}/*dpr6*^{null}
3g	*DIP-α*^{null}/*DIP-α*^{null}, 47G08LexA-LexAop-myrtdTomato/+; +/+
3h	w'; 47G08LexA-LexAop-myrtdTomato/+; *dpr6*^{null}/*dpr6*^{null}
3i	*w*; 47G08LexA-lexAopmyrtdTom/+; *dpr6*^{null}, *dpr10*$^{-8F}$/*dpr6-10*^{L}
3j	*w*; 47G08LexA-lexAopmyrtdTom/+; *dpr6*^{null}, *dpr10*$^{-20F}$/*dpr6-10*^{L}
3k	*w*; 47G08LexA-lexAopmyrtdTom/+; *dpr6*^{null}, *dpr10*$^{-40F}$/*dpr6-10*^{L}
3l	*w*; 47G08LexA-lexAopmyrtdTom/+; *dpr6-10*^{L}/*dpr6-10*^{L}

3m (from left to right)	*w;;* *DIP-α*$^{-20F}$/*DIP-α*^{null}, 47G08LexA-LexAop-myrtdTomato/+; +/+ *DIP-α*$^{-50F}$/*DIP-α*^{null}, 47G08LexA-LexAop-myrtdTomato/+; +/+ *DIP-α*$^{-20F}$/*DIP-α*^{null}, 47G08LexA-LexAop-myrtdTomato/+; dpr6/dpr6 *DIP-α*$^{-50F}$/*DIP-α*^{null}, 47G08LexA-LexAop-myrtdTomato/+; dpr6/dpr6 *DIP-α*^{null}/*DIP-α*^{null}, 47G08LexA-LexAop-myrtdTomato/+; +/+ w'; 47G08LexA-LexAop-myrtdTomato/+; *dpr6*^{null}/*dpr6*^{null} *w*; 47G08LexA-lexAopmyrtdTom/+; *dpr6*^{null}, *dpr10*$^{-8F}$/*dpr6-10*^{L} *w*; 47G08LexA-lexAopmyrtdTom/+; *dpr6*^{null}, *dpr10*$^{-20F}$/*dpr6-10*^{L} *w*; 47G08LexA-lexAopmyrtdTom/+; *dpr6*^{null}, *dpr10*$^{-40F}$/*dpr6-10*^{L} *w*; 47G08LexA-lexAopmyrtdTom/+; *dpr6-10*^{L}/*dpr6-10*^{L}
3n (from left to right)	*w;;* *DIP-α*$^{-20F}$/*DIP-α*^{null}, 47G08LexA-LexAop-myrtdTomato/+; +/+ *DIP-α*$^{-50F}$/*DIP-α*^{null}, 47G08LexA-LexAop-myrtdTomato/+; +/+ *DIP-α*$^{-20F}$/*DIP-α*^{null}, 47G08LexA-LexAop-myrtdTomato/+; dpr6/dpr6 *DIP-α*$^{-50F}$/*DIP-α*^{null}, 47G08LexA-LexAop-myrtdTomato/+; dpr6/dpr6 *DIP-α*^{null}/*DIP-α*^{null}, 47G08LexA-LexAop-myrtdTomato/+; +/+ w'; 47G08LexA-LexAop-myrtdTomato/+; *dpr6*^{null}/*dpr6*^{null} *w*; 47G08LexA-lexAopmyrtdTom/+; *dpr6*^{null}, *dpr10*$^{-8F}$/*dpr6-10*^{L} *w*; 47G08LexA-lexAopmyrtdTom/+; *dpr6*^{null}, *dpr10*$^{-20F}$/*dpr6-10*^{L} *w*; 47G08LexA-lexAopmyrtdTom/+; *dpr6*^{null}, *dpr10*$^{-40F}$/*dpr6-10*^{L} *w*; 47G08LexA-lexAopmyrtdTom/+; *dpr6-10*^{L}/*dpr6-10*^{L}
Figure 4	
4a	*w';* 75F06LexA-lexAopmyrtdTom/+; +/+
4b	*DIP-α*$^{-20F}$/*DIP-α*^{null}, 75F06LexA-LexAop-myrtdTomato/+; +/+
4c	*DIP-α*$^{-50F}$/*DIP-α*^{null}, 75F06LexA-LexAop-myrtdTomato/+; +/+
4d	*DIP-α*^{null}/*DIP-α*^{null}, 75F06LexA-LexAop-myrtdTomato/+; +/+

4e	w'; 75F06LexA-LexAop-myrtdTomato/+; *dpr6^{null}/dpr6^{null}*
4f	*w*; 75F06LexA-lexAopmyrtdTom/+; *dpr6^{null}*, *dpr10^{-8F}/dpr6-10^{L}*
4g	*w*; 75F06LexA-lexAopmyrtdTom/+; *dpr6^{null}*, *dpr10^{-20F}/dpr6-10^{L}*
4h	*w*; 75F06LexA-lexAopmyrtdTom/+; *dpr6^{null}*, *dpr10^{-40F}/dpr6-10^{L}*
4i (from left to right)	*w';* 75F06LexA-lexAopmyrtdTom/+; +/+ *DIP-α^{-20F}/DIP-α^{null}*, 75F06LexA-LexAop-myrtdTomato/+; +/+ *DIP-α^{-50F}/DIP-α^{null}*, 75F06LexA-LexAop-myrtdTomato/+; +/+ *DIP-α^{null}/DIP-α^{null}*, 75F06LexA-LexAop-myrtdTomato/+; +/+
4j (from left to right)	*w';* 75F06LexA-lexAopmyrtdTom/+; +/+ *DIP-α^{+2F}/DIP-α^{+2F}*, 75F06LexA-LexAop-myrtdTomato/+; +/+ *DIP-α^{+10F}/DIP-α^{+10F}*, 75F06LexA-LexAop-myrtdTomato/+; +/+ *w*; 75F06LexA-lexAopmyrtdTom/+; *dpr6^{null}*, *dpr10^{-20F}/dpr6-10^{L}* *w*; 75F06LexA-lexAopmyrtdTom/+; *dpr6^{null}*, *dpr10^{-40F}/dpr6-10^{L}* *w*; 75F06LexA-lexAopmyrtdTom/+; *dpr6-10^{L}/dpr6-10^{L}*
Figure 5	
5c	w'; 75F06LexA-lexAopmyrtdTom/+; +/+
5d	*DIP-α^{+2F}/DIP-α^{+2F}*; 75F06LexA-lexAopmyrtdTom/+;+/+
5e	*DIP-α^{+10F}/DIP-α^{+10F}*; 75F06LexA-lexAopmyrtdTom/+;+/+
5f	w'; LexAopmyrtdTom/+; 47G08LexA/+
5g	*DIP-α^{+2F}/DIP-α^{+2F}*; LexAopmyrtdTom/+; 47G08LexA/+
5h	*DIP-α^{+10F}/DIP-α^{+10F}*; LexAopmyrtdTom/+; 47G08LexA/+
5i(from left to right)	*w*; 75F06LexA-lexAopmyrtdTom/+; +/+ *DIP-α^{+2F}/DIP-α^{+2F}*; 75F06LexA-lexAopmyrtdTom/+;+/+ *w*; 75F06LexA-lexAopmyrtdTom/+; *dpr6^{null}*, *dpr10^{+10F}/+* *DIP-α^{+2F}/w'*; 75F06LexA-lexAopmyrtdTom/+; *dpr6^{null}, dpr10^{+10F}*/+ *DIP-α^{null1}/DIP-α^{GAL4}*; 75F06LexA-lexAopmyrtdTom/+;+/UAS-P35
Figure 6	
6a	*w*; 75F06LexA-lexAopmyrtdTom/+; +/+
6b	*w*; 75F06LexA-lexAopmyrtdTom/+; *dpr6-10^{L}/dpr6-10^{L}*
6c	*w*; 75F06LexA-lexAopmyrtdTom/UAS-Dpr10; *dpr6-10^{L}/dpr6-10^{L}*
6d	*w*; 75F06LexA-lexAopmyrtdTom/UAS-Dpr10-^{8F}; *dpr6-10^{L}/dpr6-10^{L}*
6e	*w*; 75F06LexA-lexAopmyrtdTom/UAS-Dpr10^{-20F}; *dpr6-10^{L}/dpr6-10^{L}*
6f	*w*; 75F06LexA-lexAopmyrtdTom/UAS-Dpr10^{-40F}; *dpr6-10^{L}/dpr6-10^{L}*
6g (from left to right)	*w*; 75F06LexA-lexAopmyrtdTom/+; +/+ *w*; 75F06LexA-lexAopmyrtdTom/+; *dpr6-10^{L}/dpr6-10^{L}* *w*; 75F06LexA-lexAopmyrtdTom/UAS-Dpr10; *dpr6-10^{L}/dpr6-10^{L}*

	w; 75F06LexA-lexAopmyrtdTom/UAS-Dpr10-^{8F}; *dpr6-10^{L}/dpr6-10^{L}*
	w; 75F06LexA-lexAopmyrtdTom/UAS-Dpr10^{-20F}; *dpr6-10^{L}/dpr6-10^{L}*
	w; 75F06LexA-lexAopmyrtdTom/UAS-Dpr10^{-40F}; *dpr6-10^{L}/dpr6-10^{L}*
	w; 75F06LexA-lexAopmyrtdTom/UAS-Dpr10; *dpr6-10^{L}/+*
	w; 75F06LexA-lexAopmyrtdTom/UAS-Dpr10-^{8F}; *dpr6-10^{L}/+*
	w; 75F06LexA-lexAopmyrtdTom/UAS-Dpr10^{-20F}; *dpr6-10^{L}/+*
	w; 75F06LexA-lexAopmyrtdTom/UAS-Dpr10^{-40F}; *dpr6-10^{L}/+*
Figure 7	
7a (from left to right)	*DIP-α^{+2F}/DIP-α^{+2F}*, 75F06LexA-LexAop-myrtdTomato/+; +/+
	DIP-α^{+2F}/DIP-α^{null}, 75F06LexA-LexAop-myrtdTomato/+; +/+
	w'/w'; 75F06LexA-LexAop-myrtdTomato/+; +/+
	w'/*DIP-α^{null}*; 75F06LexA-LexAop-myrtdTomato/+; +/+
	DIP-α^{-20F}/DIP-α^{-20F}, 75F06LexA-LexAop-myrtdTomato/+; +/+
	DIP-α^{-20F}/DIP-α^{null}, 75F06LexA-LexAop-myrtdTomato/+; +/+
	DIP-α^{-50F}/DIP-α^{-50F}, 75F06LexA-LexAop-myrtdTomato/+; +/+
	DIP-α^{-50F}/DIP-α^{null}, 75F06LexA-LexAop-myrtdTomato/+; +/+
	DIP-α^{null}/DIP-α^{null}, 75F06LexA-LexAop-myrtdTomato/+; +/+
7b (from left to right)	w'; 75F06LexA-lexAopmyrtdTom/+; *dpr6-10^{L}*, 9D03Gal4/+
	w'; 75F06LexA-lexAopmyrtdTom/+; *dpr6-10^{L}*, 9D03Gal4*/dpr6-10^{L}*
	w'; 75F06LexA-lexAopmyrtdTom/UAS-Dpr10D.NV5; *dpr6-10^{L}* ,9D03Gal4*/dpr6-10^{L}*
	w'; 75F06LexA-lexAopmyrtdTom/+; *dpr6-10^{L},* 9D03Gal4*/dpr6^{-20F}*
	w'; 75F06LexA-lexAopmyrtdTom/UASDpr10D.NV5^{-20F}; *dpr6-10^{L},* 9D03Gal4*/dpr6^{-20F}*
	w'; 75F06LexA-lexAopmyrtdTom/+; *dpr6-10^{L},* 9D03Gal4*/dpr6^{-40F}*
	w'; 75F06LexA-lexAopmyrtdTom/UASDpr10D.NV5^{-40F}; *dpr6-10^{L},* 9D03Gal4*/dpr6^{-40F}*

Supplemental figures

Figure S2	
(from left to right)	wild type
	DIP-α^{+2F}
	DIP-α^{-20F}
	DIP-α^{-50F}

Figure S3	
S3a	*w′/w′;* UASmyrGFP_+;15E02Gal4_+
S3b	*DIP-α^{-20F}/DIP-α^{-20F};* UASmyrGFP_+;15E02Gal4_+
S3c	*DIP-α^{-50F}/DIP-α^{-50F};* UASmyrGFP_+;15E02Gal4_+
S3d	*DIP-α^{null1}/DIP-α^{null1};* UASmyrGFP_+;15E02Gal4_+
S3e (fromleft to right)	*w′/w′*; UASmyrGFP_+;15E02Gal4_+ *DIP-α^{-20F}/DIP-α^{null1};* UASmyrGFP_+;15E02Gal4_+ *DIP-α^{-50F}/DIP-α^{null1};* UASmyrGFP_+;15E02Gal4_+ *DIP-α^{null1}/DIP-α^{null1};* UASmyrGFP_+;15E02Gal4_+
Figure S4	
(from left to right)	w'; *w*; ; *dpr6^{null}*, *dpr10^{-8F}*/+ *w*; ; *dpr6^{null}*, *dpr10^{-20F}*/+ *w*; ; *dpr6^{null}*, *dpr10^{-40F}*/+
Figure S5	
S5a (from left to right)	*w*; 47G08LexA-lexAopmyrtdTom/+; +/+ *w*; 47G08LexA-lexAopmyrtdTom/+; *dpr6-10^{L}*/ + *w*; 47G08LexA-lexAopmyrtdTom/+; *dpr6^{null}*/ *dpr6^{null}* *w*; 47G08LexA-lexAopmyrtdTom/+; *dpr6^{null}*/ *dpr6-10^{L}* *w*; 47G08LexA-lexAopmyrtdTom/+; *dpr6^{null}*, *dpr10^{-8F}*/*dpr6^{null}*, *dpr10^{-8F}* *w*; 47G08LexA-lexAopmyrtdTom/+; *dpr6^{null}*, *dpr10^{-8F}*/*dpr6-10^{L}* *w*; 47G08LexA-lexAopmyrtdTom/+; *dpr6^{null}*, *dpr10^{-20F}*/*dpr6^{null}*, *dpr10^{-20F}* *w*; 47G08LexA-lexAopmyrtdTom/+; *dpr6^{null}*, *dpr10^{-20F}*/*dpr6-10^{L}* *w*; 47G08LexA-lexAopmyrtdTom/+; *dpr6^{null}*, *dpr10^{-40F}*/*dpr6^{null}*, *dpr10^{-40F}* *w*; 47G08LexA-lexAopmyrtdTom/+; *dpr6^{null}*, *dpr10^{-40F}*/*dpr6-10^{L}* *w*; 47G08LexA-lexAopmyrtdTom/+; *dpr10^{null}*/ *dpr10^{null}* *w*; 47G08LexA-lexAopmyrtdTom/+; *dpr10^{null}*/ *dpr6-10^{L}* *w*; 47G08LexA-lexAopmyrtdTom/+; *dpr6-10^{L}*/ *dpr6-10^{L}*
S5b (from left to right)	w'; 75F06LexA-lexAopmyrtdTom/+; *dpr6-10^{L}*, 9D03Gal4/+ w'; 75F06LexA-lexAopmyrtdTom/+; *dpr6-10^{L}*, 9D03Gal4/*dpr6-10^{L}* w'; 75F06LexA-lexAopmyrtdTom/UAS-Dpr10D.NV5; *dpr6-10^{L}*, 9D03Gal4/*dpr6-10^{L}* w'; 75F06LexA-lexAopmyrtdTom/UAS-Dpr10D.NV5^{-8F}; *dpr6-10^{L}*, 9D03Gal4/*dpr6-10^{L}* w'; 75F06LexA-lexAopmyrtdTom/UAS-Dpr10D.NV5^{-20F}; *dpr6-10^{L}*, 9D03Gal4/*dpr6-10^{L}* w'; 75F06LexA-lexAopmyrtdTom/UAS-Dpr10D.NV5^{-40F}; *dpr6-10^{L}*, 9D03Gal4/*dpr6-10^{L}*

S5c (from left to right)	w'; 75F06LexA-lexAopmyrtdTom/+; *dpr6-10^{L}*, 42F06-Gal4/+ w'; 75F06LexA-lexAopmyrtdTom/+; *dpr6-10^{L}*,42F06-Gal4/*dpr6-10^{L}* w'; 75F06LexA-lexAopmyrtdTom/UAS-Dpr10D.NV5; *dpr6-10^{L}*, 42F06-3Gal4/*dpr6-10^{L}* w'; 75F06LexA-lexAopmyrtdTom/UAS-Dpr10D.NV5^{-8F}; *dpr6-10^{L},42F06-*3Gal4/*dpr6-10^{L}* w'; 75F06LexA-lexAopmyrtdTom/UAS-Dpr10D.NV5^{-20F}; *dpr6-10^{L}*,42F06-Gal4/*dpr6-10^{L}* w'; 75F06LexA-lexAopmyrtdTom/UAS-Dpr10D.NV5^{-40F}; *dpr6-10^{L}*,42F06-3Gal4/*dpr6-10^{L}*